kyo, Japan). The limit of sensitivity was 0.25 ng/mL, and the linearity limit was 8.0 ng/mL. Serum samples were diluted 1:10,000 with assay buffer before analysis.

Quantitative Reverse-Transcription-Polymerase Chain-Reaction-Based Gene Expression

Total RNA was isolated from 100 mg of mouse WAT and 50 mg of BAT with ISOGEN (Wako Pure Chemical Co., Osaka, Japan), and cDNA synthesis was performed with a First Strand cDNA Synthesis Kit (Roche, Indianapolis, IN) using 1.0 μg of total RNA. cDNA synthesized from total RNA was evaluated in a real-time polymerase chain reaction quantitative system (Light Cycler Quick System 350S; Roche Diagnostics GmbH, Mannheim, Germany). The relative amount of mRNA was calculated with β-actin mRNA as the invariant control. The following oligonucleotide primers were used: adiponectin, CTGGAGAGAAGGGAGAGAAAGG (sense) and ACATTGGGAACAGTGACGCGGG (antisense); uncoupling protein (UCP) 1, TACCAAGCTGTGCGATGT (sense) and AAGCCCAATGATGTTCAGT (antisense); and β-actin, TTGTAACCAACTGGGACGATATGG (sense) and GATCTTGATCTTCATGGTGCTAGG (antisense).

Statistical Analysis

The statistical significance of differences between groups was assessed by unpaired Student's t test. Data are presented as means ± standard error (SE).

Results

Effects of Cold Exposure on Serum Adiponectin Concentration

First, to determine the effects of cold exposure on adiponectin synthesis and serum adiponectin concentrations, mice were exposed to cold (4 °C). Twenty-four-hour cold exposure did not affect the fat content of WAT. For example, epididymal fat weight did not differ between the two groups (Table 1). In addition, histological analysis revealed that there were no significant differences in cell diameters of white adipocytes, including subcutaneous, epididymal, mesenteric, and retroperitoneal fat tissues, between control and cold-stimulated mice (Figure 1).

Although 24-hour cold exposure did not significantly affect cell sizes in WAT, where adiponectin is mainly produced, serum adiponectin concentrations were significantly decreased in response to 24-hour cold exposure (Figure 2A). We therefore examined the time course of alterations in serum adiponectin levels in response to cold stimulation, measuring adiponectin levels at 3, 6, 9, 12, and 24 hours of cold stimulation. Serum adiponectin levels decreased gradually throughout the experiment, and the difference in serum adiponectin levels between control mice and cold-stimulated mice reached statistical significance by 24 hours (Figure 2B). These data suggest that sympathetic nerve activation is involved in the regulation of serum adiponectin levels, irrespective of white adipocyte sizes.

Body weights of 12-hour cold-stimulated mice were significantly lower than those of control mice that had been exposed to 25 °C for 12 hours, whereas those of 24-hour cold-stimulated mice had been restored to the control level (Table 1). Food intake amounts of cold-stimulated mice were significantly higher than those of control mice (Table 1). These results suggest that cold stimulation accelerates energy expenditure and that hyperphagia after 12 hours restores body weight. Serum insulin and leptin levels were increased after 24- but not 12-hour cold exposure, whereas no significant changes were seen in lipid levels. In

Table 1. Parameters of 12-hr and 24-hr cold-stimulated mice

	12 hr		24 hr	
Parameter (units)	Room temperature (n = 6)	Cold stimulation (n = 7)	Room temperature (n = 6)	Cold stimulation (n = 8)
Total body weight (g)	23.20 ± 0.18	21.38 ± 0.25*	23.83 ± 0.28	24.00 ± 0.39
Food intake (g)	ND	ND	3.46 ± 0.17	7.20 ± 0.13*
Epididymal fat weight (mg)	ND	ND	273.00 ± 11.9	268.67 ± 7.32
TG (mg/dl)	31.21 ± 5.21	25.19 ± 1.73	36.39 ± 2.88	38.31 ± 1.79
T-Chol (mg/dl)	86.88 ± 3.15	93.97 ± 2.11	82.72 ± 1.65	88.34 ± 1.19
FFA (mEq/l)	0.64 ± 0.10	0.72 ± 0.07	0.54 ± 0.029	0.21 ± 0.024*
Insulin (ng/ml)	1.20 ± 0.16	1.39 ± 0.12	1.37 ± 0.16	3.35 ± 0.77†
Leptin (ng/ml)	2.68 ± 0.18	2.22 ± 0.34	2.20 ± 0.40	4.33 ± 0.48†
Glucose (mg/dl)	160.20 ± 5.16	167.00 ± 4.09	161.00 ± 2.24	167.40 ± 4.50

Data are presented graphically as means ± standard error of the mean.
* $p < 0.01$, † $p < 0.05$ vs. control as assessed by unpaired t test.

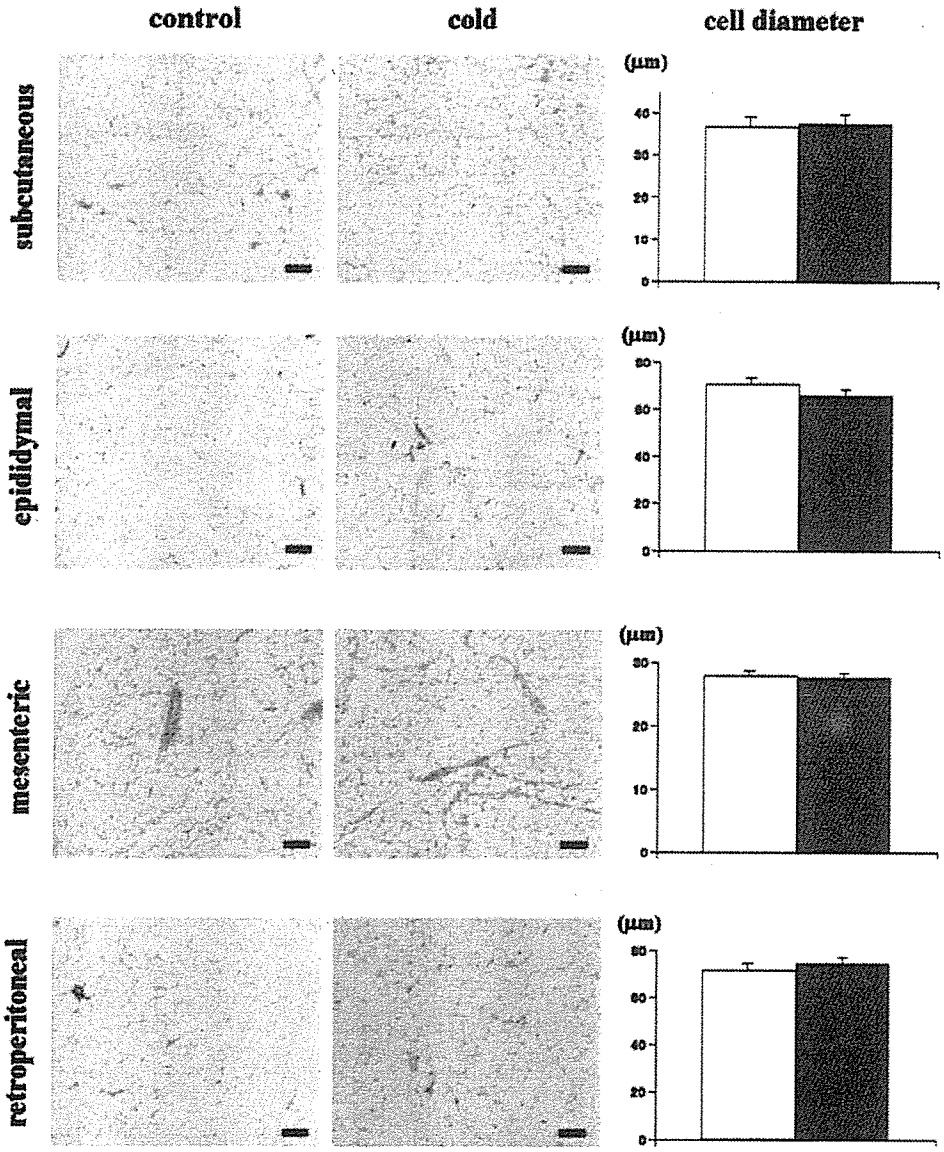

Figure 1: Effects of cold exposure on cell diameter in various WATs. Morphologies and cell diameters of adipocytes in subcutaneous, epididymal, mesenteric, and retroperitoneal fat tissues from control (white bars) and cold-stimulated (black bars) mice. Original magnification, ×100. Scale bar, 100 μm.

contrast, serum adiponectin levels were persistently decreased during cold stimulation (Figure 2B), suggesting it to be unlikely that these lipids and hormones have any major involvement in the adiponectin regulation observed in our experiments.

Next, to examine whether the serum adiponectin decrease induced by cold stimulation is due to decreased adiponectin production, we examined adiponectin mRNA expression levels in various WATs after 12- or 24-hour cold stimulation. Without cold stimulation, the adiponectin expression levels did not differ significantly among subcutaneous, mesenteric, epididymal, and retroperitoneal fat tissues (Figure 2C). Consistent with the results from the time course study of serum adiponectin levels, after 12-hour cold stimulation, adiponectin mRNA expressions in all adipose tissues examined tended to be decreased, but the differences did not reach statistical significance when compared with those in control mice. With 24-hour cold stimulation, de-

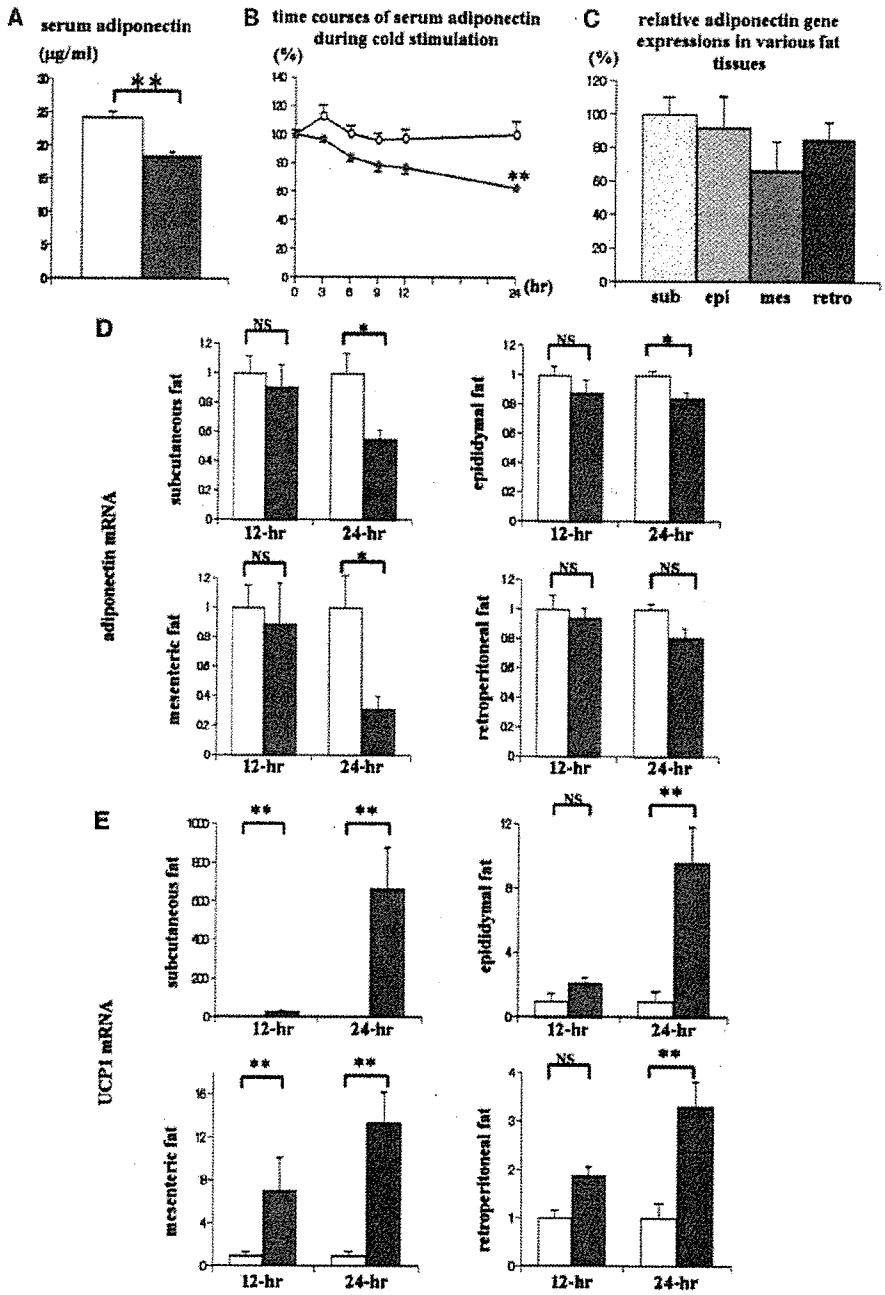

Figure 2: Effects of cold exposure on serum adiponectin concentrations, adiponectin, and UCP1 mRNA expressions in various WATs. (A) Serum adiponectin concentrations of control (open bars) and 24-hour cold-stimulated mice (gray bars) (control mice exposed to 25 °C, cold-stimulated mice to 4 °C). (B) Time courses of serum adiponectin in control (open circles) and cold-stimulated (filled circles) mice. *y*-Axis indicates percentage changes from baseline. (C) Relative adiponectin gene expressions in subcutaneous (sub), epididymal (epi), mesenteric (mes), and retroperitoneal (retro) fat. *y*-Axis indicates percent expressions of subcutaneous fat tissue. In each fat tissue, the relative amounts of adiponectin mRNA were calculated with β-actin mRNA as the invariant control. Data are presented graphically as means ± SE (n = 15 per each fat tissue). (D) Adiponectin mRNA expression levels in various WATs of control (open bars) and cold-stimulated (gray bars) mice after a 12- or 24-hour exposure to cold. (E) UCP1 mRNA expression levels in various fat tissues of control (open bars) and cold-stimulated (gray bars) mice after a 12-or 24-hour exposure to cold. Data are presented graphically as means ± SE (n = 6 per group). * $p < 0.05$ and ** $p < 0.01$ vs. control as assessed by unpaired Student's t test.

clines in adiponectin mRNA expressions in subcutaneous, epididymal, and mesenteric fat tissues became significant, whereas those in retroperitoneal fat tissue did not (Figure 2D). Thus, cold stimulation decreased adiponectin expression in various fat tissues, resulting in a decrease in serum adiponectin, although the effects of cold stimulation on adiponectin synthesis seem to differ markedly among various WATs. Taken together with the report that the number of cells in subcutaneous fat is ~75% of that in all adipose tissue of lean mice (28), adiponectin expression in subcutaneous fat is likely to contribute greatly to its serum concentration.

SNS activation reportedly increases UCP1 expression in WAT (29,30). Therefore, to investigate the degrees of activation of sympathetic nerves by various fat tissues in response to cold stimulation, we next examined UCP1 mRNA expressions in various WATs. In control mice (at 25 °C), the levels of UCP1 mRNA did not differ significantly among WATs, including subcutaneous, epididymal, mesenteric, and retroperitoneal fat (data not shown). In subcutaneous fat tissue, cold stimulation markedly increased UCP1 mRNA expression levels, 29- and 664-fold with 12- and 24-hour cold stimulation, respectively. With 12-hour cold stimulation, modest increases in UCP1 expression were observed in epididymal and mesenteric fat tissues, 2- and 7-fold; with 24-hour cold stimulation, there were further increases of 10- and 13-fold, respectively. On the other hand, the magnitude of the increment in UCP1 expression in retroperitoneal fat tissue was much smaller than those in other WATs (Figure 2E). Thus, cold stimulation activated sympathetic nerves to WATs, but the degree of the effects of cold stimulation, such as UCP1 induction, differed among WATs.

Effects of SNS Inhibitors on Serum Adiponectin Concentration after Cold Exposure

Next, to examine directly whether the serum adiponectin concentration decrease is due to SNS activation, mice were treated with α-MPT, a specific inhibitor of tyrosine hydroxylase, the rate-limiting enzyme in the synthesis of noradrenaline (31). In a previous study, to completely inhibit the SNS activation, mice were administered α-MPT intraperitoneally at a dose of 300 mg/kg body weight (24). In our preliminary study, therefore, we also administered 300 mg/kg body weight α-MPT. At this dose, however, all of the mice died during cold exposure, presumably due to diminished heat production resulting from complete blockage of SNS activation. Therefore, we administered 150 mg/kg body weight α-MPT. At this dose, ~70% of mice survived the full duration of cold exposure. We examined serum adiponectin concentrations and adiponectin expression levels in WAT using the mice that had survived throughout cold exposure. It is noteworthy that the inhibitory effects of α-MPT on SNS activation were partial, not complete.

With α-MPT administration, cold stimulation had no effect on body weights. The increment in food intake with cold stimulation was also observed in α-MPT-administered mice. Similarly, cold exposure had no impact on WAT weights (data not shown).

Serum adiponectin concentrations tended to be decreased in response to cold exposure with α-MPT administration, but the decreases were not statistically significant (Figure 3A). The magnitude of cold-exposure–induced decrements in serum adiponectin levels was significantly blunted by α-MPT administration (Figure 3B). Thus, partial inhibition of SNS activation reversed the serum adiponectin reduction, which clearly indicates involvement of SNS in regulating serum adiponectin levels. To further elucidate the mechanisms whereby SNS activation affects serum adiponectin concentrations, alterations in adiponectin mRNA levels in response to cold stimulation were examined in WAT with and without α-MPT administration. Administration of α-MPT reversed the cold-stimulation–induced decreases in adiponectin expression in subcutaneous, epididymal, and mesenteric fat tissues (Figure 3C). In retroperitoneal fat tissue, however, α-MPT administration had no effect on adiponectin expression (Figure 3C). These findings suggest that cold stimulation decreases adiponectin expression in various WATs by SNS activation, resulting in decreased serum adiponectin levels, although the degrees of the responses to cold stimulation differ markedly among WATs.

To confirm the diverse effects of SNS activation on various WATs, alterations in UCP1 mRNA levels in response to cold stimulation were examined in WAT with and without α-MPT administration. In subcutaneous fat tissue, although cold stimulation markedly enhanced UCP1 expression, this enhancement was inhibited with α-MPT administration (664- vs. 34-fold) (Figure 3D). In epididymal and mesenteric fat tissues, α-MPT administration clearly reversed the increase in UCP1 expression induced by cold stimulation (Figure 3D). In contrast, in retroperitoneal fat tissue, α-MPT administration did not significantly suppress UCP1 expression (Figure 3D). These findings indicated SNS involvement in the regulation of adiponectin expression in adipose tissues and the resultant serum adiponectin concentration, although the effects of cold stimulation were relatively small in retroperitoneal fat tissue.

Next, to determine whether β adrenergic function is involved in adiponectin regulation, mice were simultaneously administered 1.5 mg/kg body weight SR59230A, a β3 AR antagonist, and 1.5 mg/kg body weight (*S*)-(−)-propranolol, a β1/β2 AR antagonist. In a previous study, to inhibit sympathetic stimulation, these inhibitors were administered at the same doses that we used, and the effects were ana-

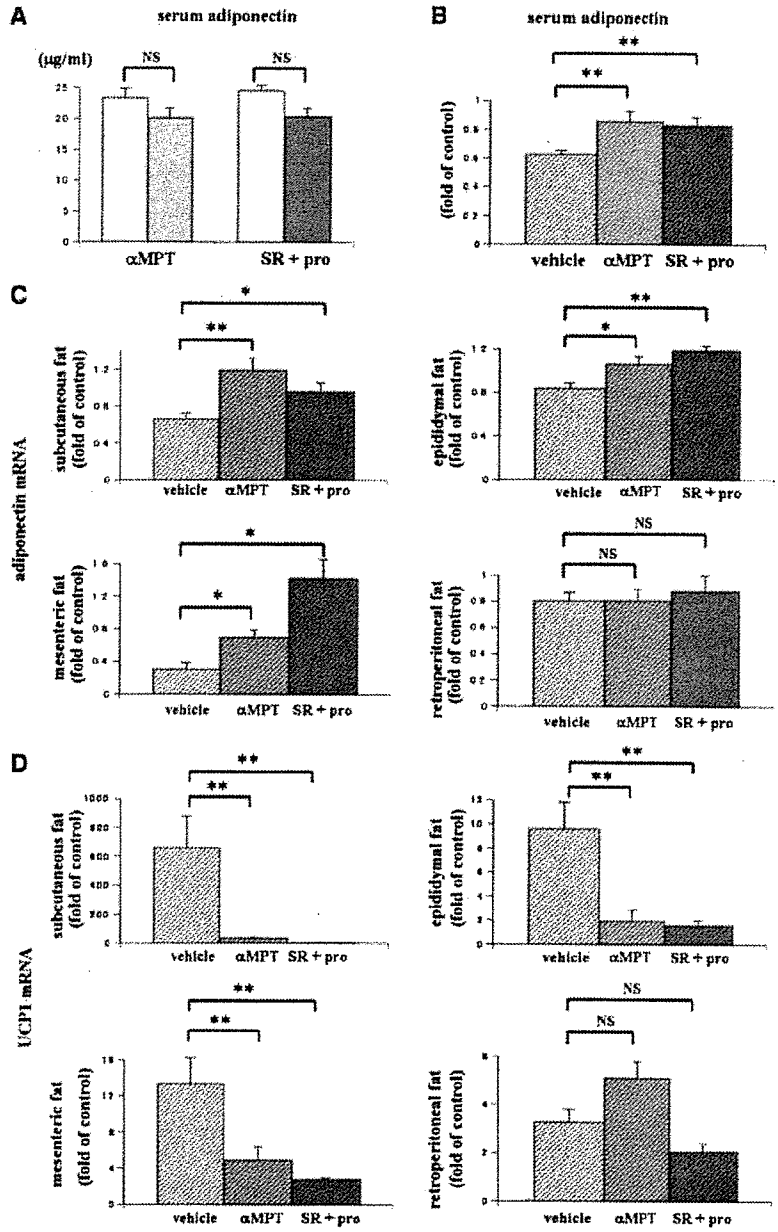

Figure 3: Effects of cold exposure with SNS inhibitor administration on serum adiponectin concentrations and adiponectin and UCP1 mRNA expressions in various WATs. (A) Serum adiponectin concentrations of control (open bar) and cold-stimulated mice given α-MPT (light gray bar) or a combination of SR59230A and propranolol (dark gray bar). Data are presented graphically as means ± SE (α-MPT-control; $n = 6$, α-MPT-cold stimulated; $n = 10$, SR + pro-control; $n = 4$, SR + pro-cold stimulated; $n = 5$). * $p < 0.05$ and ** $p < 0.01$ vs. control as assessed by unpaired Student's t test. (B) Magnitudes of serum adiponectin concentration change after cold exposure (vehicle) and those with α-MPT (α-MPT) or a combination of SR59230A and propranolol (SR + pro) administration. (C) Magnitudes of adiponectin mRNA expression changes after cold exposure (vehicle) and those with α-MPT (α-MPT) or a combination of SR59230A and propranolol (SR + pro) administration. (D) Magnitudes of UCP1 mRNA expression change after cold exposure (vehicle) and those given α-MPT (α-MPT) or a combination of SR59230A and propranolol (SR + pro). (B to D) Each parameter of 24-hour cold-stimulated mice was divided by the mean level in room-temperature-conditioned mice given the same treatment. Data are presented graphically as means ± SE (α-MPT-control, $n = 6$; α-MPT-cold-stimulated, $n = 10$; SR + pro-control, $n = 4$; SR + pro-cold-stimulated, $n = 5$). * $p < 0.05$ and ** $p < 0.01$ vs. cold exposure with vehicle.

lyzed 4 hours after administrations (32). Therefore, we administered these drugs to control and cold-stimulated mice every 4 hours for 24 hours. In our experiment, all mice survived after 24-hour cold exposure. The results were very similar to those obtained with α-MPT administration. Suppression of increased UCP1 expression in subcutaneous, epididymal, and mesenteric fat tissues confirmed effective blockade of β3 adrenergic function in these adipose tissues (Figure 3D). Adrenergic blockade inhibited the effects of cold stimulation on adiponectin expression in these fat tissues (Figure 3C) and serum adiponectin concentrations (Figure 3, A and B). In retroperitoneal fat tissue, administration of these β AR inhibitors did not significantly affect cold-exposure–induced alterations in the expression of adiponectin (Figure 3C) or UCP1 (Figure 3D). Our findings clearly show that the aforementioned adiponectin regulation by SNS is mediated mainly by β ARs. In addition, in retroperitoneal fat tissue, there appears to be little, if any, SNS involvement in metabolic activities.

Discussion

Several lines of evidence have recently suggested that adiponectin is involved in glucose and lipid metabolism. In mice, systemic adiponectin treatment increased fatty acid oxidation in muscle (33), decreased plasma glucose by enhancing the ability of insulin to suppress hepatic glucose production (34), and improved insulin sensitivity in insulin-resistant models (35). In addition, loss of the adiponectin gene in mice reportedly decreased insulin responsiveness and enhanced atherogenesis (16,36). Furthermore, a central action of adiponectin was reported: a decrease in body weight due to stimulation of energy expenditure (37). Together, these data strongly suggest that adiponectin plays an important role in preventing development of the metabolic syndrome.

Despite the physiological significance of adiponectin, the mechanism regulating serum adiponectin is still not completely understood. In the present study, cold exposure, which activates SNS physiologically, reduced adiponectin expression in various WATs, resulting in a significant decrease in the serum adiponectin concentration. In addition, administration of a noradrenaline synthesis inhibitor or β AR inhibitors inhibited cold-exposure–induced reductions in serum adiponectin levels and adiponectin expression in WATs. These findings clearly show that SNS activation, especially β stimulation, is involved in regulating the production of adiponectin and its serum levels. There is considerable evidence that adiponectin correlates negatively with body weight (9–11). In addition, adiponectin expression is reportedly decreased in enlarged adipocytes (38). However, in the present study, it is noteworthy that body weights and adipocyte sizes did not differ, regardless of 24-hour cold exposure and/or SNS inhibitor administration. These findings indicate that, independently of alterations in adiposity, SNS regulates adiponectin production and the resultant serum adiponectin levels.

Peroxisome proliferator activator (PPAR) γ reportedly increases adiponectin expression in WAT (39). However, in this study, no significant alterations were observed in PPARγ mRNA expression in various WATs of mice subjected to cold stimulation (data not shown), suggesting that cold-stimulated alteration of adiponectin mRNA expression in WAT is not mediated by increased PPARγ expression.

In contrast to our study, Puerta et al. (22) reported that, in rats, acute cold exposure did not significantly change adiponectin expression in WAT or the serum adiponectin concentration. The reasons for this discrepancy are not known, but differences in the magnitude and periods of cold exposure might explain the differing results. In our study, mice were exposed to 4 °C for 24 hours, whereas in the previous report, rats were subjected to milder cold stimulation, i.e., 6 °C for 18 hours. Alternatively, mice might be more sensitive to cold stimulation than rats. In any case, in the present study, administering a noradrenaline synthesis inhibitor or β AR inhibitors reversed the effects of cold stimulation, confirming involvement of SNS, especially β adrenergic function, in the regulation of adiponectin synthesis in WAT. Because it is well known that SNS is activated in obese subjects (40,41), decreased serum adiponectin levels in obese subjects might be, at least partly, attributable to SNS hyperactivity.

Another interesting finding in this study is the markedly different degrees of responsiveness to cold exposure among WATs. In response to cold stimulation, in subcutaneous fat tissue, UCP1 expression was increased 664-fold. In contrast, in retroperitoneal fat tissue, the increase was only 3- to 4-fold, although without cold stimulation, the UCP1 mRNA levels did not differ significantly among these WATs. In addition, although SNS inhibitor administration reversed the increases in UCP1 expression in subcutaneous, epididymal, and mesenteric fat tissues, such inhibitors did not affect UCP1 expression in retroperitoneal fat tissue. Furthermore, in contrast to other fat tissues studied, the decrease in adiponectin expression after cold exposure was not significant in retroperitoneal fat tissue. Thus, the metabolic alteration induced by SNS activation differs markedly among various fat tissues and is especially small in retroperitoneal fat tissue.

The differences in responsiveness among various WATs might be explained by how abundant the nerve supply to these fat tissues is. Alternatively, sympathetic nerves to retroperitoneal fat might not be fully activated by cold stimulation. Differential activations of SNS innervating different tissues, in response to various stimuli, have reportedly been observed. For instance, in contrast to cold stimulation, intracerebroventricular injection of 2-deoxyglucose, which activates many sympathetic nerves, suppresses the activation of sympathetic nerves to BAT (42). In addition, it

was recently reported that hypothalamic phosphoinositide 3-kinase and mitogen-activated protein kinase differentially regulate different regional sympathetic activations in response to intracerebroventricular injection of insulin (43). In the present study, we recognized that responsiveness to cold stimulation differs mechanistically among various WATs according to anatomical location. Although further studies are necessary for elucidating the mechanisms in detail, the different responses to SNS stimulation might be involved in the diverse characteristics of adipocytes according to anatomical location. Increased adiposity in various fat tissues contributes in different ways to the development of the metabolic syndrome (44,45), which might, at least in part, be explained by the magnitude of activation of sympathetic nerves to each fat tissue.

Acknowledgments

We thank I. Sato, K. Kawamura and M. Hoshi for technical support. This work was supported by a Grant-in-Aid for Scientific Research (B2, 15390282 to H.K.) and by a Grant-in-Aid for Exploratory Research (15659214 to H.K.) from the Ministry of Education, Science, Sports, and Culture of Japan and by a Grant-in-Aid for Scientific Research (H16 genome-003 to Y.O.) from the Ministry of Health, Labor, and Welfare of Japan. This work was also supported by the 21st Century COE Program Special Research Grant "the Center for Innovative Therapeutic Development for Common Diseases" from the Ministry of Education Science, Sports, and Culture (to Y.O.).

References

1. **Kahn BB, Flier JS.** Obesity and insulin resistance. *J Clin Invest.* 2000;106:473–81.
2. **Bluher M, Kratzsch J, Paschke R.** Plasma levels of tumor necrosis factor-alpha, angiotensin II, growth hormone, and IGF-I are not elevated in insulin-resistant obese individuals with impaired glucose tolerance. *Diabetes Care.* 2001;24: 328–34.
3. **Hotamisligil GS.** The role of TNFalpha and TNF receptors in obesity and insulin resistance. *J Intern Med.* 1999;245:621–5.
4. **Shimomura I, Funahashi T, Takahashi M, et al.** Enhanced expression of PAI-1 in visceral fat: possible contributor to vascular disease in obesity. *Nat Med.* 1996;2:800–3.
5. **Scherer PE, Williams S, Fogliano M, Baldini G, Lodish HF.** A novel serum protein similar to C1q, produced exclusively in adipocytes. *J Biol Chem.* 1995;270:26746–9.
6. **Hu E, Liang P, Spiegelman BM.** AdipoQ is a novel adipose-specific gene dysregulated in obesity. *J Biol Chem.* 1996;271: 10697–703.
7. **Maeda K, Okubo K, Shimomura I, Funahashi T, Matsuzawa Y, Matsubara K.** cDNA cloning and expression of a novel adipose specific collagen-like factor, apM1 (AdiPose Most abundant Gene transcript 1). *Biochem Biophys Res Commun.* 1996;221:286–9.
8. **Nakano Y, Tobe T, Choi-Miura NH, Mazda T, Tomita M.** Isolation and characterization of GBP28, a novel gelatin-binding protein purified from human plasma. *J Biochem (Tokyo).* 1996;120:803–12.
9. **Arita Y, Kihara S, Ouchi N, et al.** Paradoxical decrease of an adipose-specific protein, adiponectin, in obesity. *Biochem Biophys Res Commun.* 1999;257:79–83.
10. **Yang WS, Lee WJ, Funahashi T, et al.** Weight reduction increases plasma levels of an adipose-derived anti-inflammatory protein, adiponectin. *J Clin Endocrinol Metab.* 2001;86: 3815–9.
11. **Weyer C, Funahashi T, Tanaka S, et al.** Hypoadiponectinemia in obesity and type 2 diabetes: close association with insulin resistance and hyperinsulinemia. *J Clin Endocrinol Metab.* 2001;86:1930–5.
12. **Okamoto Y, Kihara S, Ouchi N, et al.** Adiponectin reduces atherosclerosis in apolipoprotein E-deficient mice. *Circulation.* 2002;106:2767–70.
13. **Ouchi N, Kihara S, Arita Y, et al.** Adipocyte-derived plasma protein, adiponectin, suppresses lipid accumulation and class A scavenger receptor expression in human monocyte-derived macrophages. *Circulation.* 2001;103:1057–63.
14. **Yamauchi T, Kamon J, Waki H, et al.** Globular adiponectin protected ob/ob mice from diabetes and ApoE-deficient mice from atherosclerosis. *J Biol Chem.* 2003;278:2461–8.
15. **Hotta K, Funahashi T, Arita Y, et al.** Plasma concentrations of a novel, adipose-specific protein, adiponectin, in type 2 diabetic patients. *Arterioscler Thromb Vasc Biol.* 2000;20: 1595–9.
16. **Kubota N, Terauchi Y, Yamauchi T, et al.** Disruption of adiponectin causes insulin resistance and neointimal formation. *J Biol Chem.* 2002;277:25863–6.
17. **Li H, Matheny M, Tumer N, Scarpace PJ.** Aging and fasting regulation of leptin and hypothalamic neuropeptide Y gene expression. *Am J Physiol.* 1998;275:E405–11.
18. **Gettys TW, Harkness PJ, Watson PM.** The beta 3-adrenergic receptor inhibits insulin-stimulated leptin secretion from isolated rat adipocytes. *Endocrinology.* 1996;137:4054–7.
19. **Kumar MV, Scarpace PJ.** Differential effects of retinoic acid on uncoupling protein-1 and leptin gene expression. *J Endocrinol.* 1998;157:237–43.
20. **Bradley RL, Cheatham B.** Regulation of ob gene expression and leptin secretion by insulin and dexamethasone in rat adipocytes. *Diabetes.* 1999;48:272–8.
21. **Havel PJ.** Role of adipose tissue in body-weight regulation: mechanisms regulating leptin production and energy balance. *Proc Nutr Soc.* 2000;59:359–71.
22. **Puerta M, Abelenda M, Rocha M, Trayhurn P.** Effect of acute cold exposure on the expression of the adiponectin, resistin and leptin genes in rat white and brown adipose tissues. *Horm Metab Res.* 2002;34:629–34.
23. **Trayhurn P, Duncan JS, Rayner DV.** Acute cold-induced suppression of ob (obese) gene expression in white adipose tissue of mice: mediation by the sympathetic system. *Biochem J.* 1995;311:729–33.
24. **Rayner DV, Simon E, Duncan JS, Trayhurn P.** Hyperleptinaemia in mice induced by administration of the tyrosine hydroxylase inhibitor alpha-methyl-*p*-tyrosine. *FEBS Lett.* 1998;429:395–8.

25. **Fasshauer M, Klein J, Neumann S, Eszlinger M, Paschke R.** Adiponectin gene expression is inhibited by beta-adrenergic stimulation via protein kinase A in 3T3-L1 adipocytes. *FEBS Lett.* 2001;507:142–6.
26. **Delporte ML, Funahashi T, Takahashi M, Matsuzawa Y, Brichard SM.** Pre- and post-translational negative effect of beta-adrenoceptor agonists on adiponectin secretion: in vitro and in vivo studies. *Biochem J.* 2002;367:677–85.
27. **Yoda M, Nakano Y, Tobe T, Shioda S, Choi-Miura NH, Tomita M.** Characterization of mouse GBP28 and its induction by exposure to cold. *Int J Obes Relat Metab Disord.* 2001;25:75–83.
28. **Trayhurn P, James WP, Gurr MI.** Studies on the body composition, fat distribution and fat cell size and number of "Ad," a new obese mutant mouse. *Br J Nutr.* 1979;41:211–21.
29. **Bouillaud F, Ricquier D, Mory G, Thibault J.** Increased level of mRNA for the uncoupling protein in brown adipose tissue of rats during thermogenesis induced by cold exposure or norepinephrine infusion. *J Biol Chem.* 1984;259:11583–6.
30. **Nagase I, Yoshida T, Kumamoto K, et al.** Expression of uncoupling protein in skeletal muscle and white fat of obese mice treated with thermogenic beta 3-adrenergic agonist. *J Clin Invest.* 1996;97:2898–904.
31. **Moore KE, Dominic JA.** Tyrosine hydroxylase inhibitors. *Fed Proc.* 1971;30:859–70.
32. **Evans BA, Agar L, Summers RJ.** The role of the sympathetic nervous system in the regulation of leptin synthesis in C57BL/6 mice. *FEBS Lett.* 1999;444:149–54.
33. **Fruebis J, Tsao TS, Javorschi S, et al.** Proteolytic cleavage product of 30-kDa adipocyte complement-related protein increases fatty acid oxidation in muscle and causes weight loss in mice. *Proc Natl Acad Sci USA.* 2001;98:2005–10.
34. **Berg AH, Combs TP, Du X, Brownlee M, Scherer PE.** The adipocyte-secreted protein Acrp30 enhances hepatic insulin action. *Nat Med.* 2001;7:947–53.
35. **Yamauchi T, Kamon J, Waki H, et al.** The fat-derivedhormone adiponectin reverses insulin resistance associated with both lipoatrophy and obesity. *Nat Med.* 2001;7:941–6.
36. **Maeda N, Shimomura I, Kishida K, et al.** Diet-induced insulin resistance in mice lacking adiponectin/ACRP30. *Nat Med.* 2002;8:731–7.
37. **Qi Y, Takahashi N, Hileman SM, et al.** Adiponectin acts in the brain to decrease body weight. *Nat Med.* 2004;10:524–9.
38. **Yang X, Jansson PA, Nagaev I, et al.** Evidence of impaired adipogenesis in insulin resistance. *Biochem Biophys Res Commun.* 2004;317:1045–51.
39. **Iwaki M, Matsuda M, Maeda N, et al.** Induction of adiponectin, a fat-derived antidiabetic and antiatherogenic factor, by nuclear receptors. *Diabetes.* 2003;52:1655–63.
40. **Scherrer U, Randin D, Tappy L, Vollenweider P, Jequier E, Nicod P.** Body fat and sympathetic nerve activity in healthy subjects. *Circulation.* 1994;89:2634–40.
41. **Alvarez GE, Beske SD, Ballard TP, Davy KP.** Sympathetic neural activation in visceral obesity. *Circulation.* 2002;106:2533–6.
42. **Egawa M, Yoshimatsu H, Bray GA.** Effects of 2-deoxy-D-glucose on sympathetic nerve activity to interscapular brown adipose tissue. *Am J Physiol.* 1989;257:R1377–85.
43. **Rahmouni K, Morgan DA, Morgan GM, et al.** Hypothalamic PI3K and MAPK differentially mediate regional sympathetic activation to insulin. *J Clin Invest.* 2004;114:652–8.
44. **Pouliot MC, Despres JP, Nadeau A, et al.** Visceral obesity in men: associations with glucose tolerance, plasma insulin, and lipoprotein levels. *Diabetes.* 1992;41:826–34.
45. **Abate N, Garg A, Peshock RM, Stray-Gundersen J, Grundy SM.** Relationships of generalized and regional adiposity to insulin sensitivity in men. *J Clin Invest.* 1995;96:88–98.

FEBS Letters 580 (2006) 5635–5640

WFS1 protein modulates the free Ca^{2+} concentration in the endoplasmic reticulum

Daisuke Takei[a], Hisamitsu Ishihara[a,*], Suguru Yamaguchi[a], Takahiro Yamada[a], Akira Tamura[a], Hideki Katagiri[b], Yoshio Maruyama[c], Yoshitomo Oka[a]

[a] *Division of Molecular Metabolism and Diabetes, Tohoku University Graduate School of Medicine, 2-1 Seiryo-machi, Aoba-ku, Sendai 980-8575, Japan*
[b] *Division of Advanced Therapeutics for Metabolic Diseases, Tohoku University Graduate School of Medicine, Sendai 980-8575, Japan*
[c] *Department of Physiology, Tohoku University Graduate School of Medicine, Sendai 980-8575, Japan*

Received 29 June 2006; revised 20 August 2006; accepted 5 September 2006

Available online 15 September 2006

Edited by Felix Wieland

Abstract **The *WFS1* gene, encoding an endoplasmic reticulum (ER) membrane glycoprotein, is mutated in Wolfram syndrome characterized by diabetes mellitus and optic atrophy. Herein, Ca^{2+} dynamics were examined in WFS1-knockdown and -overexpressing HEK293 cells. Studies using ER-targeted Ca^{2+}-sensitive photoprotein aequorin demonstrated WFS1 protein to positively modulate ER Ca^{2+} levels by increasing the rate of Ca^{2+} uptake. Furthermore, Ca^{2+} imaging with Fura-2 showed the magnitude of the store-operated Ca^{2+} entry to parallel WFS1 expression levels. These data indicate that WFS1 protein participates in the regulation of cellular Ca^{2+} homeostasis, at least partly, by modulating the filling state of the ER Ca^{2+} store.**

Keywords: Wolfram syndrome; WFS1; Endoplasmic reticulum; Cellular Ca^{2+} homeostasis

1. Introduction

Ca^{2+} signals control various biological functions [1] and, thus, impaired cellular Ca^{2+} homeostasis underlies a wide variety of human diseases [2]. The endoplasmic reticulum (ER), which constitutes the main intracellular Ca^{2+} store, plays a central role in Ca^{2+} homeostasis. The ER releases Ca^{2+} in response to external stimuli through the inositol 1,4,5-trisphosphate receptor and by a process of Ca^{2+}-induced Ca^{2+} release [3]. In addition, changes in intraluminal Ca^{2+} concentrations of the ER ($[Ca^{2+}]_{er}$) regulate Ca^{2+} influx through the plasma membrane, a process known as store-operated Ca^{2+} (SOC) entry [4]. Furthermore, Ca^{2+} in the ER also plays important roles in the functions, such as protein folding, of this organelle. The activities of several ERresident chaperone proteins are Ca^{2+}-dependent. Thus, a decrease in $[Ca^{2+}]_{er}$ causes misfolding of ER resident proteins, accumulation of which triggers the so-called ER stress response in the cell, leading to apoptosis in severe cases [5].

Wolfram syndrome, an autosomal recessive disorder characterized by juvenile-onset diabetes mellitus and optic atrophy [6], is caused by mutations in the *WFS1* gene [7,8]. WFS1 protein, also called wolframin, consisting of 890 amino acids, is a type II membrane protein with 9 putative transmembrane segments [9] and localizes in the ER [10]. Lack of distinct domain structures in WFS1 protein makes it difficult to identify its functions. We [11] and others [12] recently established mutant mice with a disrupted *wfs1* gene and found that these mice exhibited impaired glucose homeostasis. In *wfs1*-deficient β-cells, glucose-stimulated elevation of the cytosolic Ca^{2+} concentration ($[Ca^{2+}]_{cyt}$) was impaired [11], and the ER-stress response was persistently activated [13]. In addition, wolframin expression reportedly conferred cation channel activity and increased $[Ca^{2+}]_{cyt}$ levels in *Xenopus* oocytes [14]. These data suggested WFS1 protein to play a role in cellular Ca^{2+} homeostasis and regulation of ER functions. Herein, by analyzing WFS1-knockdown and -overexpressing HEK293 cells, we show that WFS1 protein modulates $[Ca^{2+}]_{er}$ by positively regulating the ER Ca^{2+} uptake, which is associated with changes in the $[Ca^{2+}]_{cyt}$ response evoked by Ca^{2+} store depletion.

2. Materials and methods

2.1. Generation of WFS1-knockdown and -overexpressing HEK293 cell clones

The human H1 promoter containing two *tet* operator sequences (Fig. 1A) was generated by PCR. A DNA fragment encoding short hairpin RNA (shRNA) against human *WFS1* 2254–2274 nt (GAGGAGCTCTGTCGCCTTAAG) were generated by PCR. HEK293-TRex cells (Invitrogen) were transfected with the shRNA expressing plasmid and selected against hygromycin (200 μg/ml). Two independent clones were analyzed but data obtained with clone #36 which had the highest knockdown efficiency are presented. To establish WFS1-overexpressing clones, wild-type human WFS1 cDNA was subcloned into a pTRE-Tight vector (Clontech). HEK293-rtTA cells (Clontech) were then transfected with the pTRE-Tight derivative. Two independent clones were analyzed but data obtained with clone #31 with the tightest inducibility by doxycycline (Dox, 2 μg/ml) are presented. It should be noted that WFS1-knockdown and -overexpressing cells are based on different HEK293 cell transformants,

*Corresponding author. Fax: +81 22 717 7612.
E-mail addresses: hisamitsu-ishihara@mail.tains.tohoku.ac.jp, ishihara-tky@umin.ac.jp (H. Ishihara).

Abbreviations: $[Ca^{2+}]_{cyt}$, cytosolic Ca^{2+} concentration; $[Ca^{2+}]_{er}$, ER Ca^{2+} concentration; $[Ca^{2+}]_{mt}$, mitochondrial Ca^{2+} concentration; CPA, cyclopiazonic acid; Dox, doxycycline; ER, endoplasmic reticulum; erAEQ, ER-targeted aequorin; SERCA, salco(endo)plasmic reticulum Ca^{2+} ATPase; shRNA, short hairpin RNA; SOC, store-operated Ca^{2+}; TG, thapsigargin

0014-5793/$32.00
doi:10.1016/j.febslet.2006.09.007

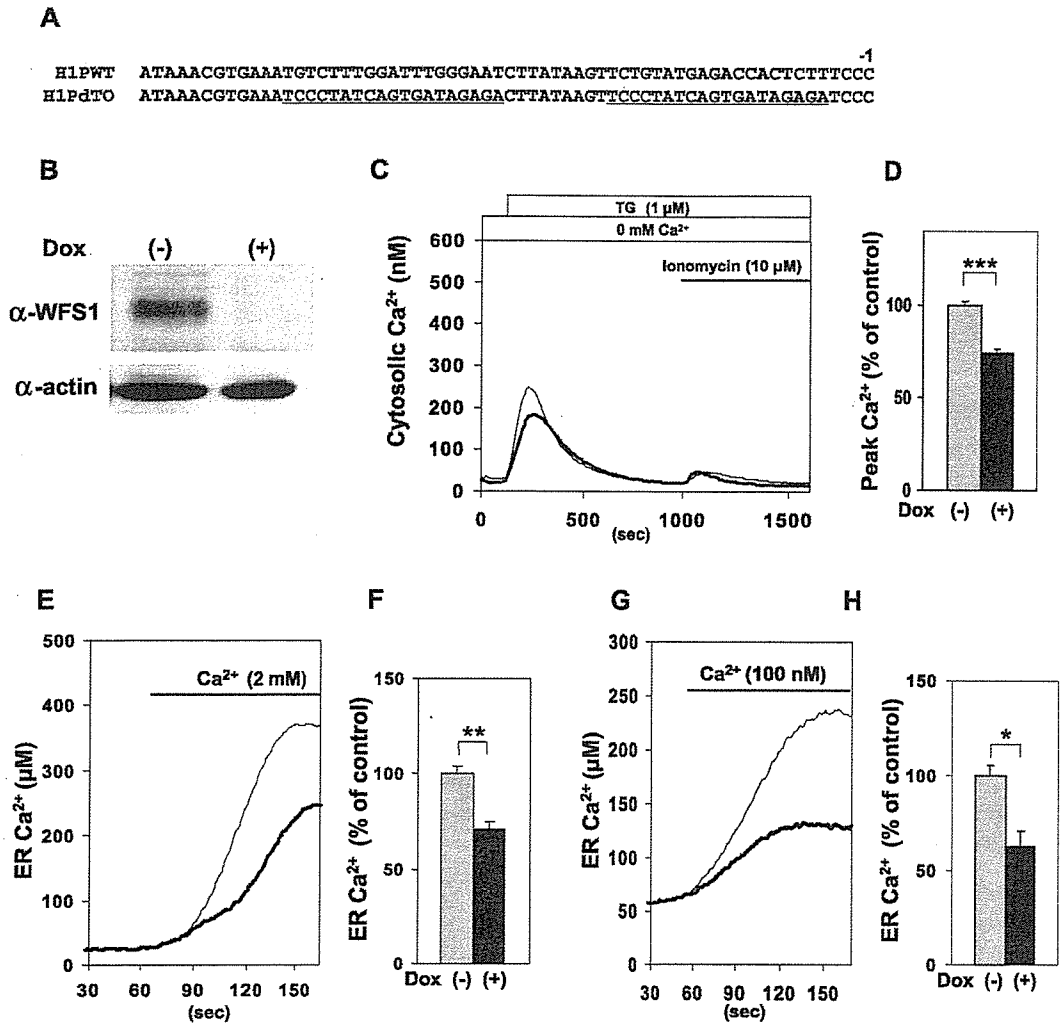

Fig. 1. Reduced ER Ca^{2+} concentrations in WFS1-knockdown cells. (A) A part of sequence of the modified human H1 promoter (H1PdTO) containing two *tet*-operator sequences (underlined) is aligned with the wild-type H1 promoter (H1PWT). (B) Expression of WFS1 protein was knocked down in HEK293 cells expressing shRNA against the *WFS1* transcript by treatment with Dox (2 μg/ml) for 3 days. (C) Cells loaded with Fura-2 were perfused in Ca^{2+}-free solution, and TG (1 μM) was then added, followed by ionomycin (10 μM). Small and comparable ionomycin-induced Ca^{2+} rises indicated that TG efficiency for emptying ER Ca^{2+} were similar between control and WFS1-knockdown cells. Traces are averages of 37 control (thin line) and 41 knockdown (thick line) cells from 3 experiments. (D) Peak amplitudes of TG-induced $[Ca^{2+}]_{cyt}$ were quantified. Gray bar, control cells ($n = 37$); Black bar, WFS1-knockdown cells ($n = 41$). (E) $[Ca^{2+}]_{er}$ in WFS1-knockdown cells measured using erAEQ. Cells transfected with an erAEQ plasmid were perfused with Ca^{2+}-free solution, followed by readdition of Ca^{2+}. Traces are representative of six perfusions each of control (thin line) and WFS1-knockdown (thick line) cells. (F) Plateau $[Ca^{2+}]_{er}$ levels in control (gray bar) and WFS1-knockdown (black bar) cells are compared ($n = 6$). (G) $[Ca^{2+}]_{er}$ measured with erAEQ in permeabilized cells. Traces are representative of four perfusions each of control (thin line) and WFS1-knockdown (thick line) cells. (H) Plateau $[Ca^{2+}]_{er}$ levels in permeabilized control (gray bar) and WFS1-knockdown (black bar) cells are compared ($n = 4$). $^{*}P < 0.05$, $^{**}P < 0.01$, $^{***}P < 0.001$.

and therefore control cells differed in WFS1-knockdown and -over-expressing experiments.

2.2. Immunodetection

HEK293 cell transformants treated with or without Dox were dissolved in 1× SDS-sample buffer. Cellular lysates were subjected to SDS–PAGE and were probed with rabbit anti-WFS1 [11], anti-actin or anti-salco(endo)plasmic reticulum Ca^{2+} ATPase (SERCA)-2 antibody (Sigma). Detection was accomplished with chemiluminescence (Amersham). HEK293 cell transformants were also fixed with 4% paraformaldehyde, permeabilized, and probed with anti-WFS1 antibody. For double staining, cells were incubated with 50 nM MitoTracker Red (Molecular Probes) for 30 min at 37 °C before fixation. The fluorescent signal was observed with an FV1000 microscope system (Olympus).

2.3. Aequorin measurement

We built our own luminescence measurement apparatus using a photomultiplier (H7360-1: Hamamatsu Photonics) and a photon counting board (M8784: Hamamatsu Photonics). For measurement of $[Ca^{2+}]_{er}$, cells seeded on coverslips and transfected with ER-targeted aequorin (erAEQ) cDNA [15] were incubated in Ca^{2+}-free solution containing 2 mM EGTA and 10 μM cyclopiazonic acid (CPA) to deplete ER Ca^{2+} and erAEQ was reconstituted with 5 μM *n*-coelenterazine (Biotium) for 60 min at 4 °C. Cells on coverslips were placed on the luminescence measurement apparatus and perfused at a flow rate of 1.5 ml/min of physiological salt solution. Experiments were terminated by lysing the cells with 100 μM digitonin in Ca^{2+}-rich solution. In some cases, cells were permeabilized with a 30 s treatment with 40 μM β-escin. Cells were first perfused with an intracellular type buffer containing 1 mM EGTA (without addition of $CaCl_2$), followed by a buffer

adjusted to approximately 100 nM free Ca^{2+} (140 mM KCl, 5 mM NaCl, 7 mM $MgSO_4$, 20 mM HEPES, pH 7.0, 10 mM ATP, 10.2 mM EGTA, 1.65 mM $CaCl_2$) at 37 °C. $[Ca^{2+}]_{mt}$ was measured according to a published method [16].

2.4. Ca^{2+} imaging using Fura-2 and Mn^{2+} quench analysis

Fluorescent images of single cells loaded with 1 μM Fura-2 acetoxymethyl ester were generated by alternate excitations at 340 and 380 nm every 10 s in physiological salt solution at 25–27 °C. $[Ca^{2+}]_{cyt}$ was calculated as reported previously [17]. For Mn^{2+} quench experiments [18], cells were perfused in Ca^{2+} free solution supplemented with thapsigargin (1 μM), followed by addition of Mn^{2+} (30 μM). Single-cell images (excitation 360 nm, emission 510 nm) were then captured.

2.5. Statistical analysis

Data are presented as means ± S.E. Differences between groups were assessed by Student's *t*-test for unpaired data.

3. Results and discussion

3.1. The free Ca^{2+} concentration in the ER is reduced in WFS1-knockdown cells

We generated WFS1-knockdown HEK293 cell clones in which WFS1 protein expression was suppressed by expressing short hairpin RNA (shRNA) against the *WFS1* transcript via a doxycycline (Dox)-inducible promoter (Fig. 1A). HEK293 cells were selected because they express WFS1 protein and lack voltage-dependent Ca^{2+} channels, simplifying data interpretation. As shown in Fig. 1B, Dox-treatment caused nearly 100% knockdown of WFS1 protein expression.

We first examined the effects of WFS1-deficiency on Ca^{2+} release from the ER induced by thapsigargin (TG), an inhibitor of salco(endo)plasmic reticulum Ca^{2+} ATPase (SERCA). When WFS1-knockdown cells were challenged with TG in the absence of extracellular Ca^{2+}, $[Ca^{2+}]_{cyt}$ elevation as measured with Fura-2 was blunted in comparison with that in control cells (Fig. 1C and D), suggesting ER Ca^{2+} content to be decreased in WFS1-knockdown cells. We, thus, directly measured $[Ca^{2+}]_{er}$ using ER-targeted aequorin (erAEQ) [15] in WFS1-knockdown cells. Knockdown of WFS1 expression was associated with a $[Ca^{2+}]_{er}$ decrease (Fig. 1E and F). To investigate whether reductions in $[Ca^{2+}]_{er}$ were direct WFS1 knockdown effects on the ER, we studied the $[Ca^{2+}]_{er}$ in WFS1-knockdown cells permeabilized with β-escin. Permeabilized cells were perfused with Ca^{2+}-free intracellular type buffer, which was switched to a buffer containing the Ca^{2+} concentration of approximately 100 nM and 10 mM ATP. The $[Ca^{2+}]_{er}$ were gradually increased with 35% lower plateaus in WFS1-knockdown than in control cells (Fig. 1G and H). These data indicated the effects of WFS1 knockdown on $[Ca^{2+}]_{er}$ to not be indirect, i.e. to not occur via the plasma membrane or cytosolic factors. Importantly, the initial rate of Ca^{2+} refilling was lower in WFS1-knockdown than in control cells (Fig. 1G; 1.88 ± 0.19 vs. 1.10 ± 0.22 μM/s for control ($n = 4$) and knockdown ($n = 4$) cells, $P < 0.05$), indicating involvement of WFS1 protein in Ca^{2+} uptake by the ER.

3.2. The Ca^{2+} concentration in the ER is increased in WFS1-overexpressing cells

We also generated HEK293 cell clones Dox-dependently overexpressing wild-type WFS1 protein. Dox-treatment induced high level expression of WFS1 protein with a reticular pattern typical for ER localization (Fig. 2A). Overexpressed WFS1 protein did not colocalize with a mitochondrial marker, MitoTracker Red (Fig. 2B). When $[Ca^{2+}]_{er}$ were measured using erAEQ, $[Ca^{2+}]_{er}$ were significantly higher in WFS1-overexpressing than in control cells (Fig. 2C and D). Analysis in permeabilized cells revealed WFS1-overxpression to result in higher plateau $[Ca^{2+}]_{er}$ levels (Fig. 2E and F) and greater initial Ca^{2+} uptake rates (Fig. 2E; 1.42 ± 0.17 vs. 2.37 ± 0.21 μM/s for control ($n = 7$) and overexpressing ($n = 7$) cells, $P < 0.01$), indicating WFS1-protein to activate Ca^{2+} uptake by the ER. To gain insight into the increased $[Ca^{2+}]_{er}$ associated with WFS1 overexpression, we next studied Ca^{2+} refilling of the ER in the presence of cyclopiazonic acid (CPA), another SERCA inhibitor (Fig. 2G). Refilling of Ca^{2+} in intact WFS1-overexpressing cells was inhibited as potently as that in control cells, indicating Ca^{2+} uptake to also be mediated by the SERCA Ca^{2+} pump in WFS1-overexpressing cells. We then studied expression of SERCA2, a major isoform of SERCA in HEK293 cells, and found no difference in its expression between WFS1-overexpressing and control cells (Fig. 2H). These results suggest WFS1 protein to modulate intrinsic activity of the SERCA Ca^{2+} pump. Future studies should be designed to elucidate molecular mechanisms of interaction between SERCA and WFS1 proteins.

3.3. SOC entry is modulated in WFS1-knockdown and -overexpressing cells

ER Ca^{2+} homeostasis affects cytosolic Ca^{2+} signaling [4]. We thus studied $[Ca^{2+}]_{cyt}$ dynamics after ER Ca^{2+} depletion in WFS1-knockdown and -overexpressing cells. When cells were treated with TG in the absence of extracellular Ca^{2+}, emptying the ER Ca^{2+} store, and then readded with Ca^{2+}, $[Ca^{2+}]_{cyt}$ responses were lower in WFS1-knockdown (Fig. 3A and B) and higher in WFS1-overexpressing (Fig. 3C and D) cells, as compared to those in control cells. The muscarinic agonist carbachol is known to induce Ca^{2+} release from the ER and subsequent Ca^{2+} influx through the plasma membrane. Carbachol-induced increases in $[Ca^{2+}]_{cyt}$ in the presence of extracellular Ca^{2+}, especially during the declining phase of the Ca^{2+} transient, were also greater in WFS1-overexpressing cells (Fig. 3E).

Modulation of Ca^{2+} influx through SOC channels could be responsible for the observed Ca^{2+} responses after store depletion. Thus, Ca^{2+} influx after depletion of the ER Ca^{2+} store was directly monitored with a Mn^{2+} quench technique [18]. We found the initial Mn^{2+} quenching rates to be slower in WFS1-knockdown cells (Fig. 3F; 100 ± 3.12 vs. 70.48 ± 3.33 (arbitrary units) for control ($n = 96$) and knockdown ($n = 109$) cells, $P < 0.001$) and faster in WFS1-overexpressing cells (traces not shown, 100 ± 5.73 vs. 136.48 ± 7.64 for control ($n = 124$) and overexpressing ($n = 127$) cells, $P < 0.01$) than in control cells.

Since the uptake of Ca^{2+} by mitochondria modulates $[Ca^{2+}]_{cyt}$ [19], changes in mitochondrial Ca^{2+} uptake could theoretically be another factor affecting the $[Ca^{2+}]_{cyt}$ response in WFS1-knockdown and -overexpressing cells. Mitochondrial Ca^{2+} concentrations ($[Ca^{2+}]_{mt}$) were, thus, studied using mitochondrial-targeted aequorin upon Ca^{2+} readdition after CPA-induced store depletion. $[Ca^{2+}]_{mt}$ was essentially unaltered in WFS1-knockdown cells (Fig. 3G), although the peak $[Ca^{2+}]_{mt}$ was slightly decreased (1.26 ± 0.07 vs. 1.04 ± 0.04 μM for

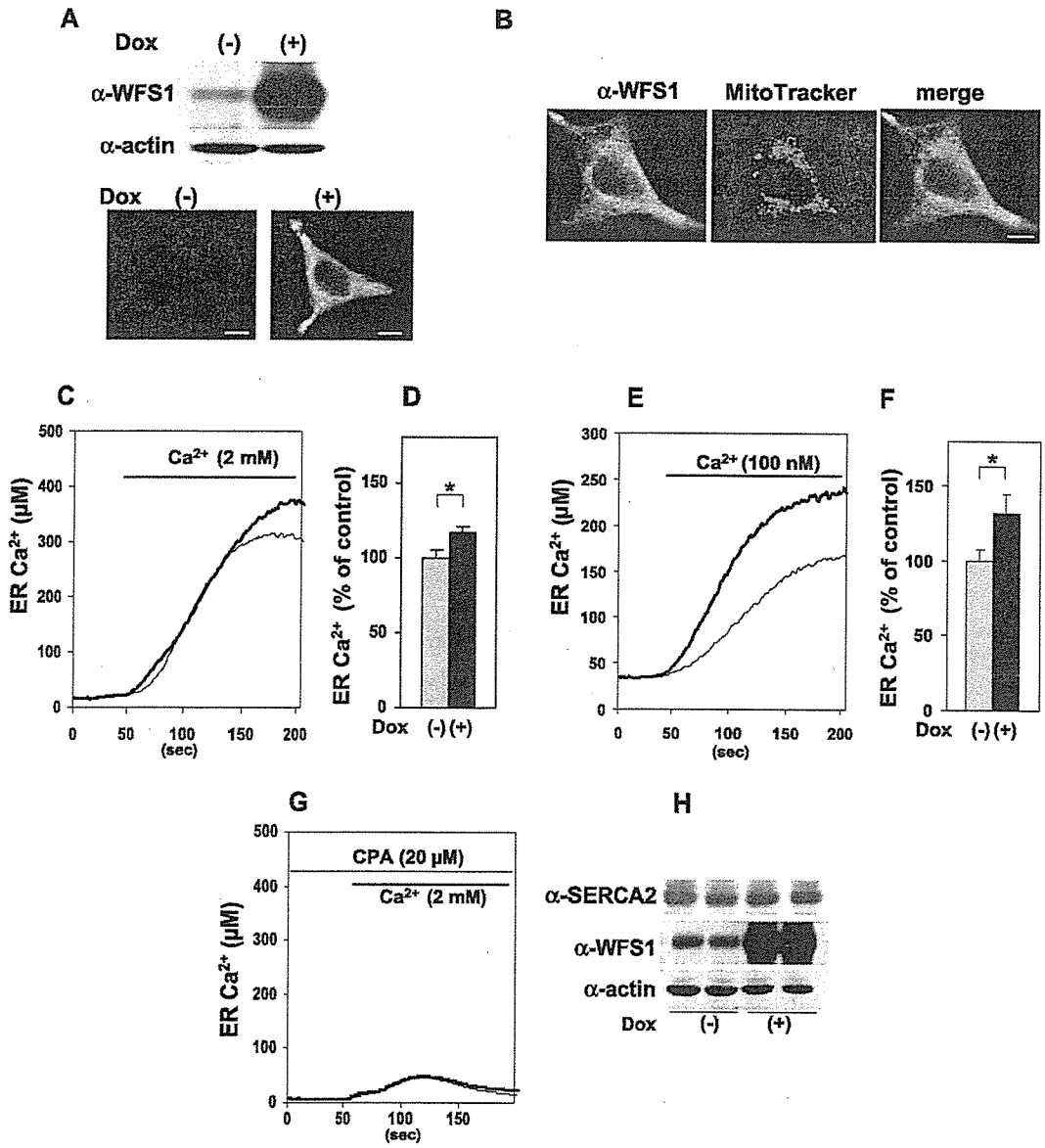

Fig. 2. Increased ER Ca^{2+} concentrations in WFS1-overexpressing cells. (A) Overexpression of WFS1 was induced by treatment with Dox (2 μg/ml) for three days. Note that our WFS1 antibody detected endogenous WFS1 on Western blotting but was not sensitive enough to detect it on immunohistochemistry in HEK293 cells. Bars, 4 μm. (B) WFS1-overexpressing cells were incubated with 50 nM MitoTracker Red before fixation and stained using an anti-WFS1-antibody. Bar, 4 μm. (C) $[Ca^{2+}]_{er}$ in WFS1-overexpressing cells. Traces are representative of 10 perfusions each of control (thin line) and WFS1-overexpressing (thick line) cells. (D) Plateau $[Ca^{2+}]_{er}$ levels in control (gray bar) and WFS1-overexpressing (black bar) cells are compared ($n = 10$). (E) $[Ca^{2+}]_{er}$ in permeabilized WFS1-overexpressing cells. Traces are representative of seven perfusions each of control (thin line) and WFS1-overexpressing (thick line) cells. (F) Plateau $[Ca^{2+}]_{er}$ levels in permeabilized control (gray bar) and WFS1-overexpressing (black bar) cells are compared ($n = 7$). (G) $[Ca^{2+}]_{er}$ measured in intact control (thin line) and WFS1-overexpressing (thick line) cells in the presence of cyclopiazonic acid (CPA). Traces are representative of three perfusions. (H) Immunoblot of SERCA2 in WFS1-overexpressing cells. The blot shown is representative of three independent experiments. $^*P < 0.05$.

control ($n = 7$) and knockdown ($n = 7$) cells, $P < 0.05$). Thus, the decrease in the $[Ca^{2+}]_{cyt}$ response in WFS1-knockdown cells was not due to an increase in mitochondrial Ca^{2+} uptake. Conversely, in WFS1-overexpressing cells, $[Ca^{2+}]_{mt}$ upon Ca^{2+} readdition was increased (Fig. 3H; 1.36 ± 0.05 vs. 1.76 ± 0.04 μM for control ($n = 7$) and overexpressing ($n = 7$) cells, $P < 0.001$), excluding the possibility of the enhanced $[Ca^{2+}]_{cyt}$ response being due to reduced Ca^{2+} uptake by mitochondria. Taken together, these data indicated altered $[Ca^{2+}]_{cyt}$ responses after depletion of ER Ca^{2+} stores in WFS1-knockdown and -overexpressing cells to be not due to changes in mitochondrial Ca^{2+} uptake but due to changes in SOC entry.

Decreased SOC entry associated with reduced ER Ca^{2+} levels was previously reported in cells overexpressing the proapoptotic protein Bcl-2 [19,20] and in cells expressing presenilin mutants linked to familial Alzheimer's disease [21]. It was suggested that a reduction in $[Ca^{2+}]_{er}$ levels decreased SOC influx by an adaptive downregulation of the pathway

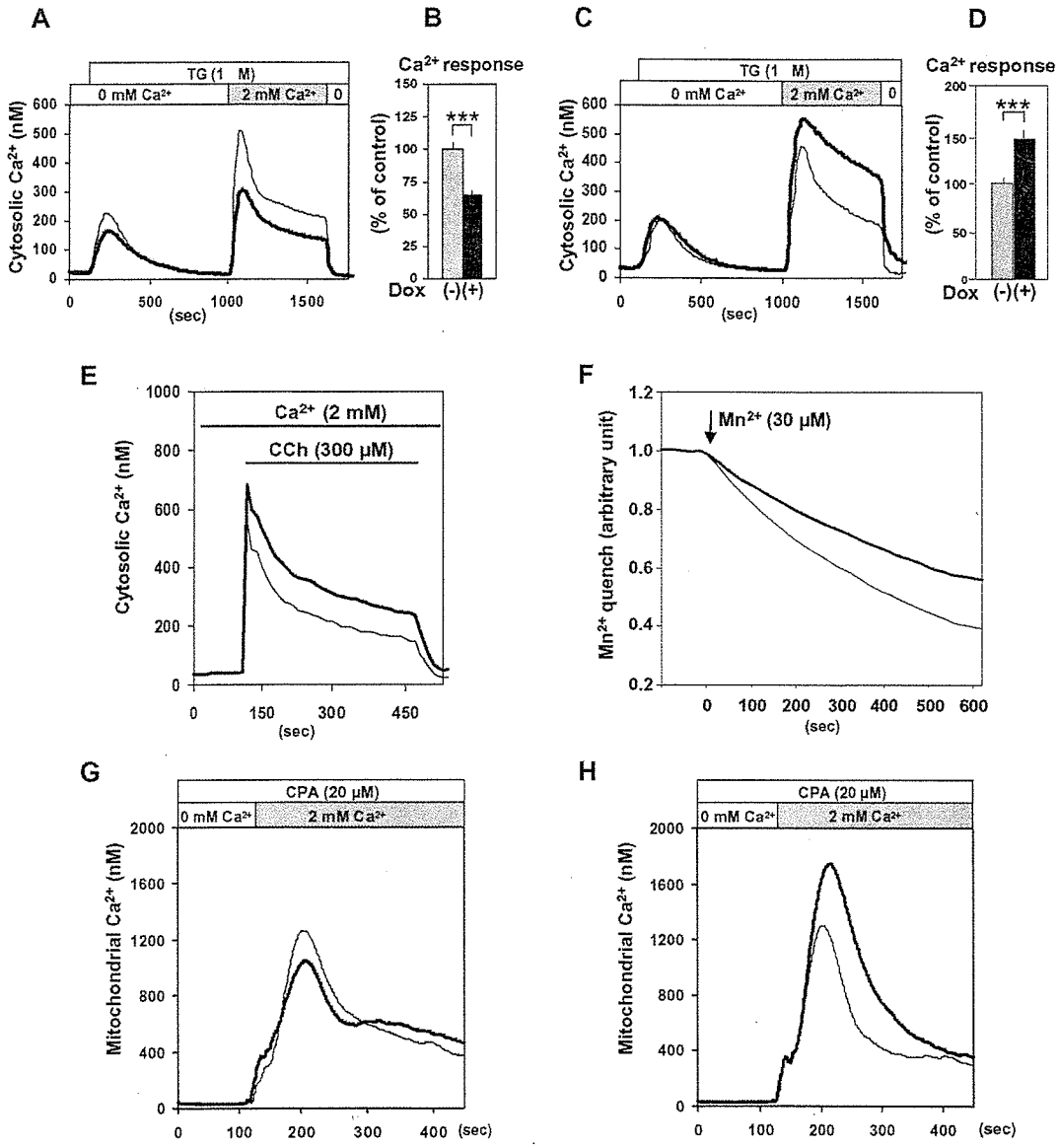

Fig. 3. Modulation of SOC entry in WFS1-knockdown and -overexpressing cells. (A) $[Ca^{2+}]_{cyt}$ responses to Ca^{2+} readdition after Ca^{2+} store depletion was analyzed with Fura-2 in control (thin line) and WFS1-knockdown (thick line) cells. Traces are averages of 62 control and 64 WFS1-knockdown cells from four experiments. (B) Areas under the curves (AUCs), in response to Ca^{2+} readdition in (A), were quantified. Gray bar, control cells ($n = 62$); Black bar, WFS1-knockdown cells ($n = 64$). (C) $[Ca^{2+}]_{cyt}$ responses to Ca^{2+} readdition after Ca^{2+} store depletion in control (thin line) and WFS1-overexpressing (thick line) cells. Traces are averages of 51 control and 65 WFS1-overexpressing cells from three experiments. (D) AUCs in response to Ca^{2+} readdition in (C) were quantified. Gray bar, control cells ($n = 51$); Black bar, WFS1-overexpressing cells ($n = 65$). (E) Carbachol-stimulated $[Ca^{2+}]_{cyt}$ increases in control (thin line: $n = 39$) and WFS1-overexpressing (thick line: $n = 40$) cells. (F) Ca^{2+} influx was evaluated by Mn^{2+} quench assay in WFS1-knockdown cells. Traces are averages of 96 control (thin line) and 109 knockdown (thick line) cells from six experiments. (G) $[Ca^{2+}]_{mt}$ responses to Ca^{2+} readdition after ER store depletion in control (thin line) and WFS1-knockdown (thick line) cells. Traces are representative of 7 perfusions. (H) $[Ca^{2+}]_{mt}$ responses to Ca^{2+} readdition after ER store depletion in control (thin line) and WFS1-overexpressing (thick line) cells. Traces are representative of seven perfusions. $^{***}P < 0.001$.

for activating SOC influx [19]. However, reduced ER Ca^{2+} levels were not always associated with a decrease in SOC entry; reduced ER Ca^{2+} levels without alteration in SOC entry were reported in BAX and BAK double-knockout cells [22]. In addition to changes in cytosolic Ca^{2+} dynamics, increased Ca^{2+} uptake into mitochondria was observed upon Ca^{2+} readdition after CPA-induced store depletion in WFS1-overexpressing cells. A simple explanation for this was that the increased Ca^{2+} uptake might be due to elevated SOC influx. Alternatively, increased $[Ca^{2+}]_{er}$ might enhance Ca^{2+} supply to the mitochondria upon store depletion and activated mitochondrial function. The close relationship between the ER and mitochondria was recently established [23], and supports this notion. Further studies are needed to clarify the relation between the ER Ca^{2+} store filling state and responses of $[Ca^{2+}]_{cyt}$ and $[Ca^{2+}]_{mt}$ in WFS1-knockdown and -overexpressing cells.

The present data indicate WFS1 protein, an enigmatic protein, to play a role in regulating cellular Ca^{2+} homeostasis, at least partly, by modifying the filling state of the ER Ca^{2+} store. Our previous results demonstrated that WFS1-deficiency causes increased ER-stress in pancreatic β-cells but not in cells from the heart, skeletal muscle or brown adipose tissues [13]. In pancreatic β-cells, which produce large quantities of insulin, there is a greater load on the ER. Impaired ER Ca^{2+} homeostasis is known to cause or exacerbate ER stress [24]. It is possible that combined effects of reduced $[Ca^{2+}]_{er}$ and a greater load on the ER induce ER stress specifically in β-cells. Our present data, thus, provide clues to elucidating not only WFS1 functions but also the molecular mechanisms underlying β-cell failure in Wolfram syndrome.

Acknowledgements: We thank Prof. T. Pozzan (University of Padua) for generously providing ER-targeted aequorin cDNA, Prof. H. Takeshima (Kyoto University) for advice on the Ca^{2+} measurements, and Dr. Kanzaki for help with confocal microscopy experiments. We are also grateful to Y. Nagura and K. Tanaka for their expert assistance. This work was supported by Grants-in-Aid for Scientific Research (17590264 to H.I. and 17390258 to Y.O.) from the Ministry of Education, Science, Sports and Culture of Japan.

References

[1] Berridge, M.J., Lipp, P. and Bootman, M.D. (2000) The versatility and universality of calcium signalling. Nat. Rev. Mol. Cell Biol. 1, 11–21.
[2] Rizzuto, R. and Pozzan, T. (2003) When calcium goes wrong: genetic alterations of a ubiquitous signaling route. Nat. Genet. 34, 135–141.
[3] Meldolesi, J. and Pozzan, T. (1998) The endoplasmic reticulum Ca^{2+} store: a view from the lumen. Trends Biochem. Sci. 23, 10–14.
[4] Parekh, A.B. and Putney Jr., J.W. (2005) Store-operated calcium channels. Physiol. Rev. 85, 757–810.
[5] Schroder, M. and Kaufman, R.J. (2005) The mammalian unfolded protein response. Annu. Rev. Biochem. 74, 739–789.
[6] Wolfram, D.J. and Wagener, H.P. (1938) Diabetes mellitus and simple optic atrophy among siblings: report on four cases. Mayo. Clinic Proc. 13, 715–718.
[7] Inoue, H., Tanizawa, Y., Wasson, J., Behn, P., Kalidas, K., Bernal-Mizrachi, E., Mueckler, M., Marshall, H., Donis-Keller, H., Crock, P., Rogers, D., Mikuni, M., Kumashiro, H., Higashi, K., Sobue, G., Oka, Y. and Permutt, M.A. (1998) A gene encoding a transmembrane protein is mutated in patients with diabetes mellitus and optic atrophy (Wolfram syndrome). Nat. Genet. 20, 143–148.
[8] Strom, T.M., Hortnagel, K., Hofmann, S., Gekeler, F., Scharfe, C., Rabl, W., Gerbitz, K.D. and Meitinger, T. (1998) Diabetes insipidus, diabetes mellitus, optic atrophy and deafness (DIDMOAD) caused by mutations in a novel gene (wolframin) coding for a predicted transmembrane protein. Hum. Mol. Genet. 7, 2021–2028.
[9] Hofmann, S., Philbrook, C., Gerbitz, K.D. and Bauer, M.F. (2003) Wolfram syndrome: structural and functional analyses of mutant and wild-type wolframin, the WFS1 gene product. Hum. Mol. Genet. 12, 2003–2012.
[10] Takeda, K., Inoue, H., Tanizawa, Y., Matsuzaki, Y., Oba, J., Watanabe, Y., Shinoda, K. and Oka, Y. (2001) WFS1 (Wolfram syndrome 1) gene product: predominant subcellular localization to endoplasmic reticulum in cultured cells and neuronal expression in rat brain. Hum. Mol. Genet. 10, 477–484.
[11] Ishihara, H., Takeda, S., Tamura, A., Takahashi, R., Yamaguchi, S., Takei, D., Yamada, T., Inoue, H., Soga, H., Katagiri, H., Tanizawa, Y. and Oka, Y. (2004) Disruption of the WFS1 gene in mice causes progressive beta-cell loss and impaired stimulus-secretion coupling in insulin secretion. Hum. Mol. Genet. 13, 1159–1170.
[12] Riggs, A.C., Bernal-Mizrachi, E., Ohsugi, M., Wasson, J., Fatrai, S., Welling, C., Murray, J., Schmidt, R.E., Herrera, P.L. and Permutt, M.A. (2005) Mice conditionally lacking the Wolfram gene in pancreatic islet beta cells exhibit diabetes as a result of enhanced endoplasmic reticulum stress and apoptosis. Diabetologia 48, 2313–2321.
[13] Yamada, T., Ishihara, H., Tamura, A., Takahashi, R., Yamaguchi, S., Takei, D., Tokita, A., Satake, C., Tashiro, F., Katagiri, H., Aburatani, H., Miyazaki, J. and Oka, Y. (2006) WFS1-deficiency increases endoplasmic reticulum stress, impairs cell cycle progression and triggers the apoptotic pathway specifically in pancreatic β-cells. Hum. Mol. Genet. 15, 1600–1609.
[14] Osman, A.A., Saito, M., Makepeace, C., Permutt, M.A., Schlesinger, P. and Mueckler, M. (2003) Wolframin expression induces novel ion channel activity in endoplasmic reticulum membranes and increases intracellular calcium. J. Biol. Chem. 278, 52755–52762.
[15] Montero, M., Brini, M., Marsault, R., Alvarez, J., Sitia, R., Pozzan, T. and Rizzuto, R. (1995) Monitoring dynamic changes in free Ca^{2+} concentration in the endoplasmic reticulum of intact cells. EMBO J. 14, 5467–5475.
[16] Rizzuto, R., Simpson, A.W., Brini, M. and Pozzan, T. (1992) Rapid changes of mitochondrial Ca^{2+} revealed by specifically targeted recombinant aequorin. Nature 358, 325–327.
[17] Grynkiewicz, G., Poenie, M. and Tsien, R.Y. (1985) A new generation of Ca^{2+} indicators with greatly improved fluorescence properties. J. Biol. Chem. 260, 3440–3450.
[18] Kass, G.E., Llopis, J., Chow, S.C., Duddy, S.K. and Orrenius, S. (1990) Receptor-operated calcium influx in rat hepatocytes: identification and characterization using manganese. J. Biol. Chem. 265, 17486–17492.
[19] Pinton, P., Ferrari, D., Magalhaes, P., Schulze-Osthoff, K., Di Virgilio, F., Pozzan, T. and Rizzuto, R. (2000) Reduced loading of intracellular Ca^{2+} stores and downregulation of capacitative Ca^{2+} influx in Bcl-2-overexpressing cells. J. Cell Biol. 148, 857–862.
[20] Foyouzi-Youssefi, R., Arnaudeau, S., Borner, C., Kelley, W.L., Tschopp, J., Lew, D.P., Demaurex, N. and Krause, K.H. (2000) Bcl-2 decreases the free Ca^{2+} concentration within the endoplasmic reticulum. Proc. Natl. Acad. Sci. USA 97, 5723–5728.
[21] Zatti, G., Burgo, A., Giacomello, M., Barbiero, L., Ghidoni, R., Sinigaglia, G., Florean, C., Bagnoli, S., Binetti, G., Sorbi, S., Pizzo, P. and Fasolato, C. (2006) Presenilin mutations linked to familial Alzheimer's disease reduce endoplasmic reticulum and Golgi apparatus calcium levels. Cell Calcium 39, 539–550.
[22] Scorrano, L., Oakes, S.A., Opferman, J.T., Cheng, E.H., Sorcinelli, M.D., Pozzan, T. and Korsmeyer, S.J. (2003) BAX and BAK regulation of endoplasmic reticulum Ca^{2+}: a control point for apoptosis. Science 300, 135–139.
[23] Rizzuto, R., Duchen, M.R. and Pozzan, T. (2004) Flirting in little space: the ER/mitochondria Ca^{2+} liaison. Sci. STKE 215, 1–9.
[24] Verkhratsky, A. and Toescu, E.C. (2003) Endoplasmic reticulum Ca^{2+} homeostasis and neuronal death. J. Cell. Mol. Med. 7, 351–361.

Original Article

Involvement of Apolipoprotein E in Excess Fat Accumulation and Insulin Resistance

Junhong Gao,[1,2] Hideki Katagiri,[2] Yasushi Ishigaki,[1] Tetsuya Yamada,[1] Takehide Ogihara,[2] Junta Imai,[1,2] Kenji Uno,[1,2] Yutaka Hasegawa,[1,2] Makoto Kanzaki,[3] Tokuo T. Yamamoto,[4] Shun Ishibashi,[5] and Yoshitomo Oka[1]

Although apolipoprotein E (apoE) is well known to play a major role in lipid metabolism, its role in glucose and energy homeostasis remains unclear. Herein, we established apoE-deficient genetically obese Ay (apoE$^{-/-}$;Ay/+) mice. ApoE deficiency in Ay mice prevented the development of obesity, with decreased fat accumulation in the liver and adipose tissues. ApoE$^{-/-}$;Ay/+ mice exhibited better glucose tolerance than apoE$^{+/+}$;Ay/+ mice. Insulin tolerance testing and hyperinsulinemic-euglycemic clamp study revealed marked improvement of insulin sensitivity, despite increased plasma free fatty acid levels. These metabolic phenotypes were reversed by adenoviral replenishment of apoE protein, indicating circulating apoE to be involved in increased adiposity and obesity-related metabolic disorders. Uptake of apoE-lacking VLDL into the liver and adipocytes was markedly inhibited, but adipocytes in apoE$^{-/-}$;Ay/+ mice exhibited normal differentiation, suggesting that apoE-dependent VLDL transport is involved in the development of obesity, i.e., surplus fat accumulation. Interestingly, apoE$^{-/-}$;Ay/+ mice exhibited decreased food intake and increased energy expenditure. Pair-feeding experiments indicate these phenomena to both contribute to the obesity-resistant phenotypes associated with apoE deficiency. Thus, apoE is involved in maintaining energy homeostasis. ApoE-dependent excess fat accumulation is a promising therapeutic target for the metabolic syndrome. *Diabetes* **56:24–33, 2007**

From the [1]Division of Molecular Metabolism and Diabetes, Tohoku University Graduate School of Medicine, Sendai, Japan; the [2]Division of Advanced Therapeutics for Metabolic Diseases, Center for Translational and Advanced Animal Research, Tohoku University Graduate School of Medicine, Sendai, Japan; the [3]Tohoku University Bio-Engineering Research Organization, Sendai, Japan; the [4]Center for Advanced Genome Research, Institute of Development, Aging and Cancer, Tohoku University, Sendai, Japan; and the [5]Division of Endocrinology and Metabolism, Department of Medicine, Jichi Medical School, Tochigi, Japan.

Address correspondence and reprint requests to Hideki Katagiri, MD, PhD, Division of Advanced Therapeutics for Metabolic Diseases, Center for Translational and Advanced Animal Research, Tohoku University Graduate School of Medicine, 2-1 Seiryo-machi, Aoba-ku, Sendai 980-8575, Japan. E-mail: katagiri@mail.tains.tohoku.ac.jp.

Received for publication 1 February 2006 and accepted in revised form 16 October 2006.

J.G., H.K., and Y.I. contributed equally to this work.

Additional information for this article can be found in an online appendix at http://diabetes.diabetesjournals.org.

ApoE, apolipoprotein E; FFA, free fatty acid; HPLC, high-performance liquid chromatography; IRS, insulin receptor substrate; TNF, tumor necrosis factor; VLDLR, VLDL receptor.

DOI: 10.2337/db06-0144

Obesity causes various metabolic disorders, including diabetes, dyslipidemia, and hypertension and has become a major public health concern in most industrialized countries in recent decades (1). Obesity results mainly from excess energy intake and physical inactivity, and the molecular mechanisms of body weight control have been intensively studied from various aspects, including appetite, energy expenditure, glucose and lipid metabolism, and adiposity (2). Excess fat accumulation is associated with metabolic disorders including insulin resistance, glucose intolerance, and dyslipidemia (3). In addition, we reported that dissipating excess energy improves diabetes and obesity in mice (4). On the other hand, lipoatrophy also leads to these metabolic disorders in mice and humans. Fat-less mice (5,6) as well as patients with lipodystrophy (7) exhibit severe insulin resistance and diabetes. Thus, having an appropriate adipose tissue amount is important for maintaining glucose homeostasis via adipocyte metabolic activities including production and secretion of adipocytokines.

Apolipoprotein E (apoE) is a structural component of all lipoprotein particles except LDL and serves as a high-affinity ligand for lipoprotein receptors (8). ApoE plays important roles in hepatic uptake of chylomicron and VLDL remnants (9,10) as well as hepatic secretion of VLDL (11). In contrast, involvement of apoE in adiposity, insulin sensitivity, and glucose metabolism is somewhat controversial. ApoE$^{-/-}$ mice treated with gold thioglucose become obese and diabetic (12). High-fat chow induces obesity in apoE$^{-/-}$ mice in a manner similar to that in wild-type C57BL/6 mice, while apoE deficiency produced resistance to some obesity-related phenotypic features, including hyperinsulinemia and hyperglycemia (13). On the other hand, Chiba et al. reported that apoE deficiency in *ob/ob* mice resulted in neither increased body weight nor adiposity, but glucose metabolism and insulin sensitivity were not examined (14). They attributed decreased adiposity in *ob/ob*;apoE$^{-/-}$ mice to impaired adipocyte differentiation based on in vitro findings obtained using bone marrow stromal cells and 3T3-L1 cells. However, impaired adipocyte differentiation induces severe insulin resistance and diabetes (5,6), markedly different from the metabolic phenotypes of apoE$^{-/-}$ mice. Thus, it remains unclear how, and even whether, apoE is involved in adiposity and glucose metabolism.

Herein, we recognized that adult apoE$^{-/-}$ mice are leaner and more glucose tolerant than wild-type mice. In contrast, younger apoE$^{-/-}$ mice exhibit normal adiposity,

i.e., they are not lipoatrophic. These findings led us to postulate that apoE is involved in surplus fat accumulation, resulting in the development of insulin resistance, but does not play a major role in the fat accumulation required for adipocyte function. To clarify whether apoE is involved in the development of insulin resistance associated with obesity and, if so, to identify the underlying mechanisms, we established apoE-deficient genetically obese Ay (apoE$^{-/-}$;Ay/+) mice. Without impairing adipocyte differentiation in vivo, apoE deficiency in Ay mice prevented obesity, glucose intolerance, and insulin resistance. Interestingly, apoE$^{-/-}$;Ay/+ mice exhibited decreased food intake and increased energy expenditure, both of which contribute to the obesity-resistant phenotypes associated with apoE deficiency. Thus, apoE is a key molecule for development of obesity, i.e., excess fat accumulation, and is a possible therapeutic target for the metabolic syndrome.

RESEARCH DESIGN AND METHODS

Animal studies were conducted in accordance with the institutional guidelines for animal experiments at Tohoku University. ApoE$^{+/-}$;Ay/+ mice were obtained by mating male KKAy mice (Nippon CLEA, Shizuoka, Japan) and female apoE-deficient mice with the C57BL/6J background (15) (The Jackson Laboratory, Bar Harbor, ME). Male apoE$^{+/-}$;Ay/+ mice were mated with female apoE$^{+/-}$ mice with the C57BL/6J background. Mice of three genotypes, apoE$^{+/+}$;Ay/+, apoE$^{+/-}$;Ay/+, and apoE$^{-/-}$;Ay/+, were selected. Littermates were used in each experiment. These mice were housed individually and started on a high-fat diet consisting of 15.3% (wt/wt) fat (Quick Fat; Nippon CLEA, Shizuoka, Japan) at 6 weeks of age. Experiments were performed 5 weeks after high-fat loading. Viruses were administered intravenously at a dose of 2×10^8 plaque-forming units 4 weeks after high-fat loading. For pair-feeding experiments, apoE$^{+/+}$;Ay/+ mice were allotted into two groups at 4 weeks of age. One group was given their daily food allotments based on the previous days' consumption by apoE$^{-/-}$;Ay/+ littermate mice.

Recombinant adenovirus preparation. Recombinant adenovirus, containing the human apoE2, E3, E4, or bacterial β-galactosidase gene (*Adex1CAlacZ*) cDNA under the CAG promoter, was prepared as described previously (16).

Oxygen consumption. Oxygen consumption was measured with an O_2/CO_2 metabolism measuring system (model MK-5000RQ; Muromachikikai, Tokyo, Japan) as described previously (4).

Histological analysis. Livers and adipose tissues were removed, fixed with 10% formalin, and embedded in paraffin. Tissue sections were stained with hematoxylin-eosin or 0.1% (wt/vol) Oil Red O. Total adipocyte areas were traced manually and analyzed. Brown and white adipocyte areas were measured in 100 or more cells per mouse in each group.

Triglyceride contents of the liver and adipose tissue. Frozen livers or adipose tissues were homogenized, and triglycerides were extracted with $CHCl_3$:CH_3OH (2:1 vol:vol), dried, and resuspended in 2-propanol. Triglyceride contents were measured using Lipidos liquid (Toyobo, Osaka, Japan).

Tyrosine phosphorylation of insulin receptor substrate 1. Mice that had been fasted for 16 h were injected with 100 μl normal saline (0.9% NaCl), with or without 10 units/kg body wt of insulin via the tail vein. Hindlimb muscles were removed 300 s later and immediately homogenized. After centrifugation, the resulting supernatants were used for immunoprecipitation with anti-insulin receptor substrate 1 (IRS-1) antibody (17). Immunoprecipitates were subjected to SDS-PAGE and then immunoblotted using antiphosphotyrosine antibody (4G10) as described previously (17).

Blood analysis. Blood glucose, plasma insulin, leptin, adiponectin, tumor necrosis factor (TNF)-α, total cholesterol, triglyceride, and free fatty acid (FFA) concentrations were determined as described previously (4). Plasma lipoproteins were analyzed by high-performance liquid chromatography (HPLC) using molecular sieve columns (Skylight Biotech, Akita, Japan) (18).

Glucose and insulin tolerance tests. Glucose and insulin tolerance tests were performed as described previously with slight modification (19). Glucose tolerance tests were performed on fasted (10 h) mice. Mice were given oral glucose (1 g/kg body wt), and blood glucose was assayed immediately before and at 15, 30, 60, and 120 min postadministration. Insulin tolerance tests were performed on fed mice. Mice were injected with human regular insulin (1.5 units/kg body wt; Eli Lilly, Kobe, Japan) into the intraperitoneal space, and blood glucose was assayed immediately before and at 20, 40, 60, and 80 min postinjection.

Hyperinsulinemic-euglycemic clamp. Hyperinsulinemic-euglycemic clamp studies were performed as described previously (20). Chronically cannulated, conscious and unrestrained mice were fasted for 6 h before the study. Insulin (500 mU · kg^{-1} · min^{-1}) was infused throughout the clamp study. Blood glucose was monitored every 5 min via carotid arterial catheter samples. Glucose was infused at a variable rate to maintain blood glucose at 120 mg/dl. The glucose infusion rate and endogenous glucose production were calculated as described (20).

Quantitative RT-PCR–based gene expression. Total RNA was isolated from 0.1 g mouse adipose tissue with Isogen (Wako Pure Chemical, Osaka, Japan), and cDNA was synthesized with a Cloned AMV First Strand Synthesis Kit (Invitrogen, Rockville, MD) using 5 μg total RNA. cDNA synthesized from total RNA was evaluated using real-time quantitative PCR (Light Cycler Quick System 350S; Roche Diagnostics, Mannheim, Germany). The relative amount of mRNA was calculated with 28S rRNA as the invariant control. The primers used are described in Supplemental Table 1 (online appendix [available at http://diabetes.diabetesjoumals.org]).

β-VLDL uptake into cultured adipocytes. Murine 3T3-L1 preadipocytes were maintained and differentiated into adipocytes as described previously (21). β-VLDL ($d < 1.006$ g/ml) was purified from the blood of apoE$^{-/-}$ mice with high-fat loading and labeled with fluorescent lipid DiI (1,1′-dioctadecyl-3,3,3′,3′-tetramethylindocarbocyanine perchlorate) as described previously (22). After labeling with DiI, β-VLDL was incubated with an equal amount of recombinant human apoE3 for 1 h at 37°C (23). DiI-labeled β-VLDL (4 μg protein/ml) with or without apoE had been incubated with fully differentiated 3T3-L1 adipocytes for 8 h at 37°C. Cells were rinsed twice with PBS and solubilized with 0.1 N NaOH/1% SDS. Fluorescent intensities of cell lysates were measured with a fluorescent spectrophotometer (F-2000; Hitachi, Tokyo, Japan) (24).

Triglyceride secretion rate. To assess hepatic triglyceride secretion, 500 mg/kg Triton WR-1339 (Sigma), which blocks lipolysis of triglycerides in peripheral tissue, was injected into the tail veins of the 6 h–fasted apoE$^{+/+}$;Ay/+ mice, and blood samples were taken immediately before and 30, 60, and 90 min after injection (25).

Hepatic uptake of β-VLDL. Male C57BL/6N mice at 6 weeks of age were injected via tail vein with fluorescent β-VLDL (5 μg/mouse) with or without apoE in 0.2 ml PBS. Thirty minutes after injection, the mice were killed and their livers excised for lipid extraction and fluorescence measurement as described previously (26).

Statistical analysis. All data were expressed as means ± SEM. The statistical significance of differences was assessed by the unpaired *t* test and one-factor ANOVA.

RESULTS

ApoE deficiency inhibited the development of obesity. This study was prompted by the unexpected observation that aged apoE$^{-/-}$ mice are leaner and more insulin sensitive than apoE$^{+/+}$ mice of the same age with the C57BL/6J background. Therefore, we weighed apoE$^{-/-}$ and apoE$^{+/+}$ mice from 6 to 42 weeks of age, while maintaining the animals on high-fat chow. Body weights were similar through 10 weeks of age, but apoE$^{-/-}$ mice had significantly lower body weights after 14 weeks of age (Fig. 1*A*). Glucose tolerance in 30-week-old apoE$^{-/-}$ mice was moderately better than that in apoE$^{+/+}$ littermate mice (Fig. 1*B*). Thus, apoE deficiency prevents the development of obesity and associated glucose intolerance, while its effects on glucose tolerance are small.

Next, to elucidate the roles of apoE in development of the metabolic disorders associated with obesity, we established apoE$^{+/+}$;Ay/+, apoE$^{+/-}$;Ay/+, and apoE$^{-/-}$;Ay/+ mice. These mice were fed a 15% fat chow from 6 weeks of age. First, we compared body weights. As shown in Fig. 1*C*, mice gained weight in an apoE gene dosage-dependent manner; apoE deficiency significantly suppressed weight gain. Several organs and tissues were weighed at 11 weeks of age. Weights of the liver and both brown and white adipose tissues were significantly lower in an apoE gene dosage-dependent manner (Fig. 1*D*). In contrast, weights of other organs, which are minimally involved in lipid accumulation, were similar in apoE$^{+/+}$;Ay/+ and apoE$^{-/-}$;Ay/+ mice (Supplemental Table 2 [online appendix]). Triglyceride contents of the liver and mesenteric adipose

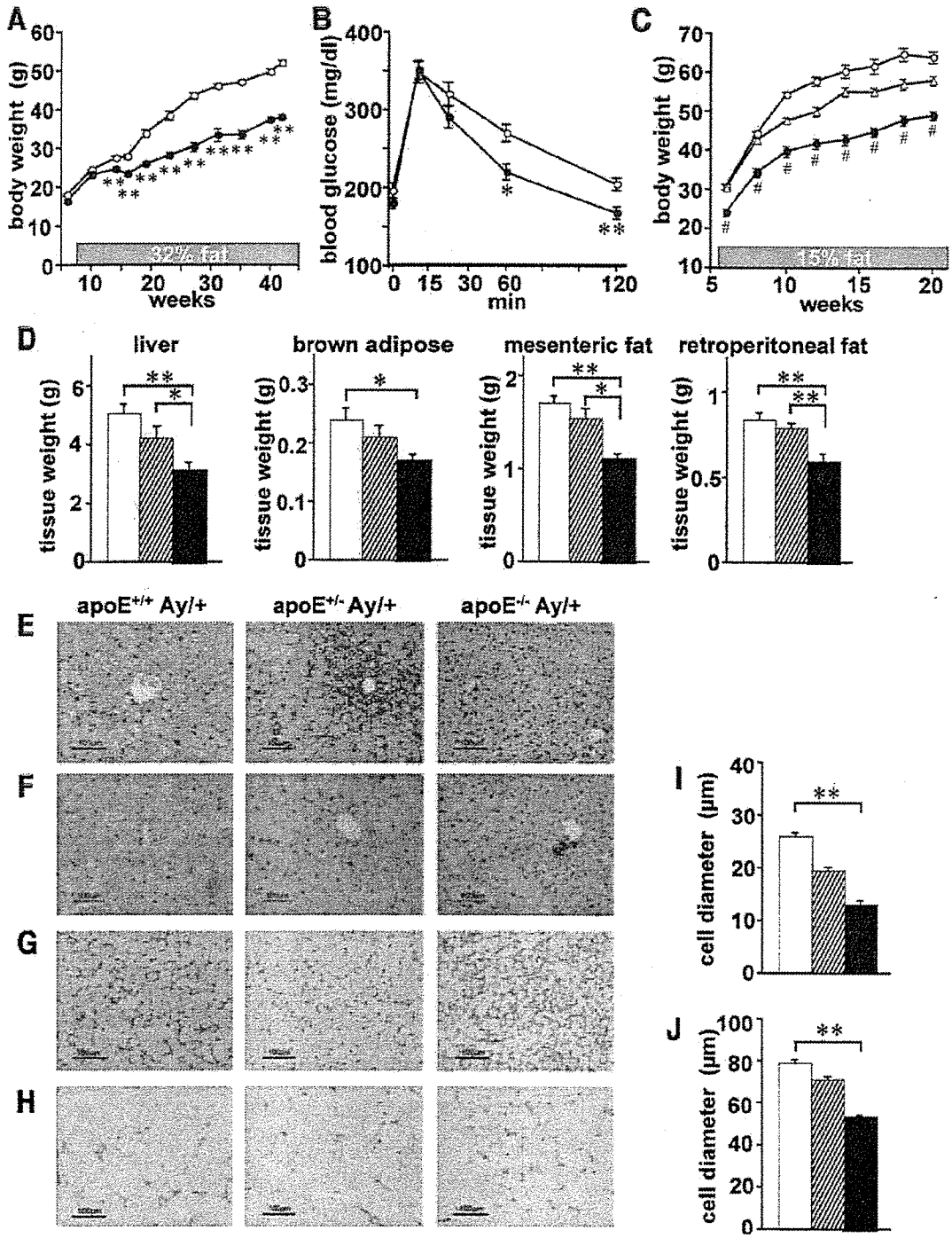

FIG. 1. ApoE deficiency suppressed body weight gain and fat accumulation. *A* and *B*: Body weights were determined from 6 to 40 weeks of age (*A*) and glucose tolerance tests were performed (*B*) in apoE$^{+/+}$ mice (○) and apoE$^{-/-}$ mice (●; n = 6 per group) at 30 weeks of age with the C57BL/6 background. *C*: Body weights were determined from 6 to 20 weeks of age in apoE$^{+/+}$;Ay/+ (○), apoE$^{+/-}$;Ay/+ (△), and apoE$^{-/-}$;Ay/+ (●) mice fed 15% fat chow. *D–J*: The liver and fat tissues of apoE$^{+/+}$;Ay/+, apoE$^{+/-}$;Ay/+, and apoE$^{-/-}$;Ay/+ mice at 11 weeks of age. *D*: The liver, brown adipose, and mesenteric and retroperitoneal white adipose tissues from apoE$^{+/+}$;Ay/+ (□), apoE$^{+/-}$;Ay/+ (▨), and apoE$^{-/-}$;Ay/+ (■) mice (n = 6–8 per group) were weighed. *E–J*: Histological findings of the liver stained with hematoxylin-eosin (*E*) and Oil Red O (*F*), as well as hematoxylin-eosin staining of brown adipose (*G*) and mesenteric white adipose (*H*) tissues in apoE$^{+/+}$;Ay/+ (*left*), apoE$^{+/-}$;Ay/+ (*middle*), and apoE$^{-/-}$;Ay/+ (*right*) mice. Brown adipose (*I*) and mesenteric white adipose (*J*) cell diameters were measured in apoE$^{+/+}$;Ay/+ (□), apoE$^{+/-}$;Ay/+ (▨), and apoE$^{-/-}$;Ay/+ (□) mice. Representative histological findings are shown. Data are presented as means ± SE. *$P < 0.05$, **$P < 0.01$ by the unpaired t test and one-way ANOVA.

tissue were significantly smaller in apoE$^{-/-}$;Ay/+ than in apoE$^{+/+}$;Ay/+ mice (apoE$^{+/+}$;Ay/+ vs. apoE$^{-/-}$;Ay/+ mice: liver, 0.467 ± 0.069 vs. 0.365 ± 0.036 mg/protein, P = 0.02; white adipose tissue, 12.4 ± 1.4 vs. 5.8 ± 1.3 mg/protein, P = 0.002). Histological analyses revealed that apoE deficiency inhibited hepatic fat accumulation, while abundant lipid droplets were present in the livers of apoE$^{+/+}$;Ay/+ mice (Fig. 1*E* and *F*). In addition, brown

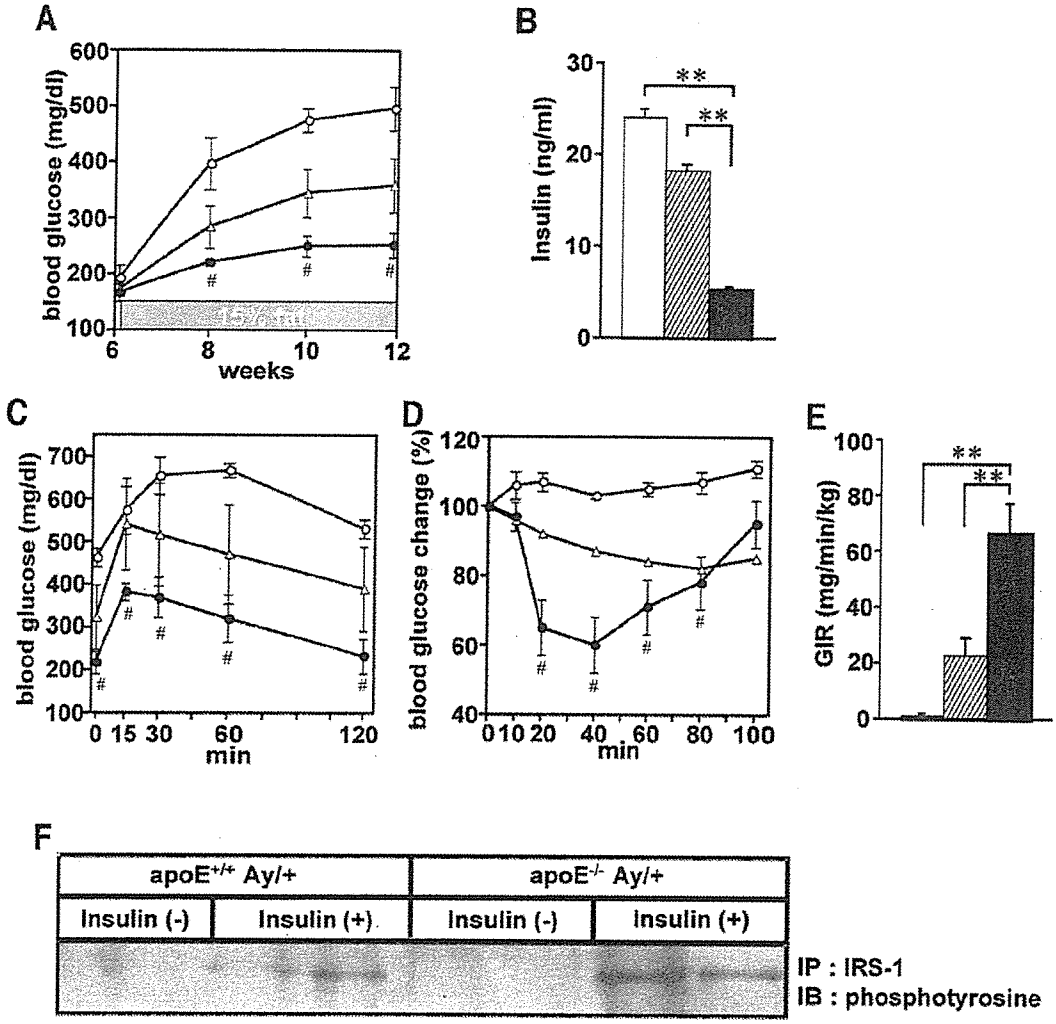

FIG. 2. ApoE deficiency improved glucose tolerance and insulin sensitivity in genetically obese mice. *A*: Fasting blood glucose levels were examined in apoE$^{+/+}$;Ay/+ (○), apoE$^{+/-}$;Ay/+ (△), and apoE$^{-/-}$;Ay/+ (●) mice biweekly from 6 to 12 weeks of age. *B*: Fasting plasma insulin levels of apoE$^{+/+}$;Ay/+ (□), apoE$^{+/-}$;Ay/+ (▨), and apoE$^{-/-}$;Ay/+ (■) mice were measured. *C* and *D*: Glucose tolerance (*C*) and insulin tolerance (*D*) tests were performed in apoE$^{+/+}$;Ay/+ (○), apoE$^{+/-}$;Ay/+ (△), and apoE$^{-/-}$;Ay/+ (●) mice. Data were expressed as percentages of blood glucose levels immediately before intraperitoneal insulin loading (n = 4–6 per group). *E*: Glucose infusion rates during hyperinsulinemic-euglycemic clamp studies were measured in apoE$^{+/+}$;Ay/+ (□), apoE$^{+/-}$;Ay/+ (▨), and apoE$^{-/-}$;Ay/+ (■) mice (n = 3 per group). *F*: Insulin-stimulated tyrosine phosphorylation of IRS-1 proteins in muscle. Mice that had been fasted for 16 h received an intravenous injection of 100 μl normal saline with or without insulin (10 units/kg body wt). Hindlimb muscles were removed 300 s later, and lysates were immunoprecipitated with anti–IRS-1 antibody. Immunoprecipitates were subjected to SDS-PAGE and immunoblotted with anti-phosphotyrosine antibody (4G10). Representative histological findings and immunoblots are presented. These metabolic studies in *B–F* were performed using 11-week-old mice. In *A–E*, data are presented graphically as means ± SE. *P < 0.05, **P < 0.01 by the unpaired t test and one-way ANOVA.

(Fig. 1*G*) and white (Fig. 1*H*) adipose tissues of apoE$^{-/-}$;Ay/+ mice were significantly smaller than those of apoE$^{+/+}$;Ay/+ mice. ApoE deficiency also decreased cell diameters in both brown (Fig. 1*I*) and white (Fig. 1*J*) adipose tissues. These findings suggest that apoE deficiency results in resistance to obesity via suppression of fat accumulation in the liver and fat tissues under obesity-inducing conditions.

ApoE deficiency induced greater glucose tolerance and insulin sensitivity in obese states. As described previously (15), lipid metabolism was markedly impaired with apoE deficiency (Supplemental Fig. 1*A* [online appendix]). Plasma cholesterol, triglyceride, and FFA levels were markedly higher in apoE$^{-/-}$;Ay/+ than in apoE$^{+/+}$;Ay/+ mice. HPLC analysis of plasma lipid profiles revealed that chylomicron, VLDL, and LDL fractions were markedly increased in apoE$^{-/-}$;Ay/+ compared with apoE$^{+/+}$;Ay/+ mice (Supplemental Fig. 1*B* [online appendix]).

Next, we examined the effects of apoE deficiency on glucose metabolism as well as insulin sensitivity in genetically obese Ay mice. From age 8 weeks onward, fasting blood glucose was markedly increased in apoE$^{+/+}$;Ay/+ mice on high-fat chow, but this glucose elevation was significantly inhibited by apoE deficiency (Fig. 2*A*). Fasting blood insulin levels at 11 weeks of age were lower, by 78%, in apoE$^{-/-}$;Ay/+ than in apoE$^{+/+}$;Ay/+ mice (Fig. 2*B*). Glucose (Fig. 2*C*) and insulin (Fig. 2*D*) tolerance tests documented that apoE$^{-/-}$;Ay/+ mice were more glucose tolerant and insulin sensitive. We further examined insulin sensitivity using hyperinsulinemic-euglycemic clamp procedures. apoE$^{+/+}$;Ay/+ mice fed high-fat chow exhibited severe insulin resistance, while in apoE$^{-/-}$;Ay/+ mice, glucose infusion rates were markedly higher, by 54-fold (Fig. 2*E*). Thus, despite hyperlipidemia, especially increased plasma FFA levels, apoE deficiency markedly

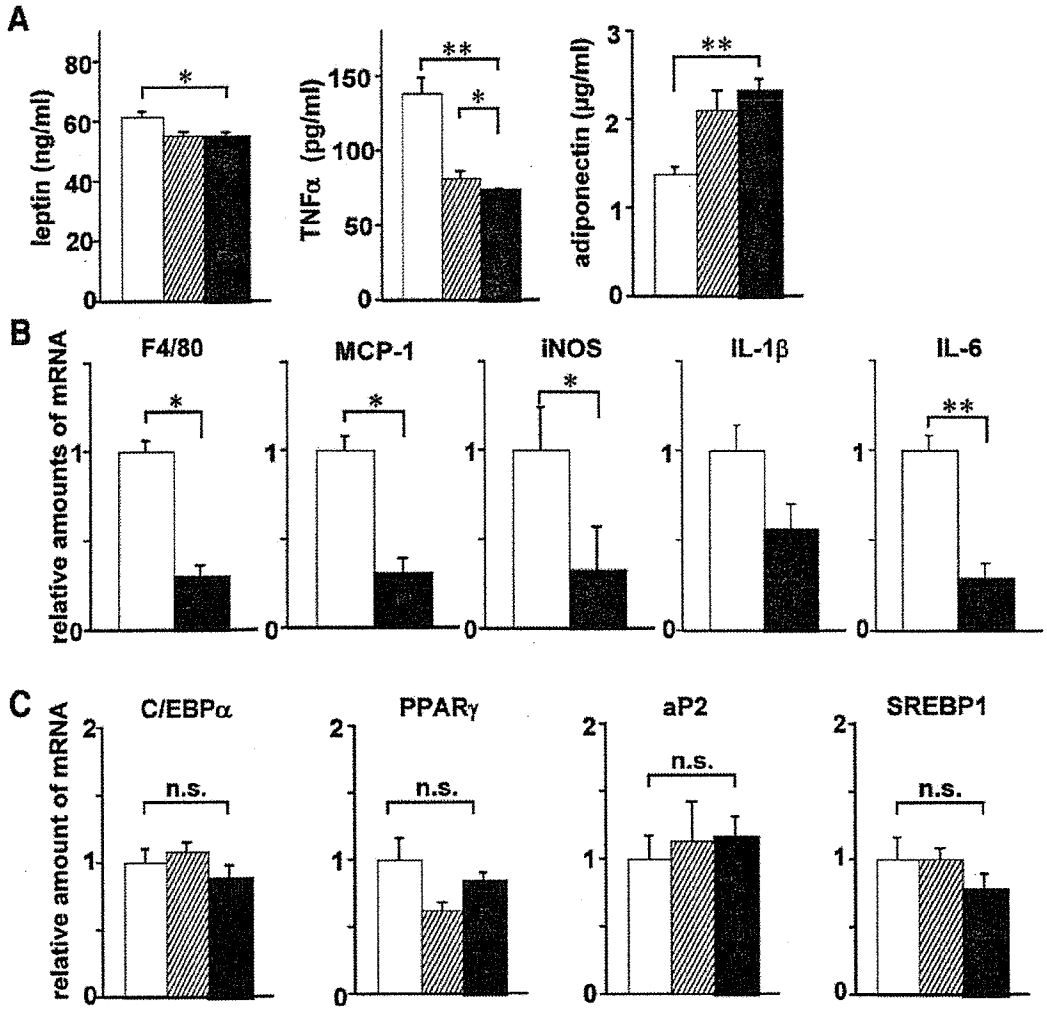

FIG. 3. ApoE deficiency affected plasma adipocytokine profiles and expressions of the mRNAs for inflammation- and differentiation-related proteins in adipose tissue. *A*: Plasma adipocytokines (*left*, leptin; *middle*, TNF-α; *right*, adiponectin) of high-fat chow–fed apoE$^{+/+}$;Ay/+ (□), apoE$^{+/-}$;Ay/+ (▨), and apoE$^{-/-}$;Ay/+ (■) mice were measured after a 10-h fast at 11 weeks of age. *B* and *C*: Relative amounts of mRNA in mesenteric white adipose tissue from apoE$^{+/+}$;Ay/+ (□) and apoE$^{-/-}$;Ay/+ (■) mice were determined by quantitative RT-PCR and corrected with 28S rRNA as the internal standard. Total RNA in white adipose tissue was isolated, after a 10-h fast, from 11-week-old mice. Levels of the mRNA levels for inflammation (*B*)- and differentiation (*C*)-related proteins in adipose tissue were assayed (n = 6 per group). Data are presented as means ± SE. *P < 0.05, **P < 0.01 by one-way ANOVA (*A*) and the unpaired t test (*B* and *C*).

improves glucose tolerance and insulin sensitivity. In addition, insulin-stimulated tyrosine phosphorylation of IRS-1 in muscle was enhanced in apoE$^{-/-}$;Ay/+ compared with apoE$^{+/+}$;Ay/+ mice (Fig. 2*F*). Thus, apoE deficiency apparently prevents surplus fat accumulation in adipose tissue and insulin resistance in muscle, resulting in better glucose tolerance.

Adipocytes are differentiated normally in apoE$^{-/-}$;Ay/+ mice in vivo. We next determined plasma adipocytokine profiles (Fig. 3*A*). In apoE$^{-/-}$;Ay/+ mice, plasma leptin levels were slightly decreased and TNF-α levels were markedly lower than those in apoE$^{+/+}$;Ay/+ mice, while plasma adiponectin levels were significantly higher. Thus, apoE deficiency improved obesity-induced alterations in adipocytokine profiles. In addition, quantitative RT-PCR revealed that expressions of F4/80, monocyte chemoattractant protein-1, inducible nitric oxide synthase, and interleukin-6 in mesenteric adipose tissue were significantly lower in apoE$^{-/-}$;Ay/+ than in apoE$^{+/+}$;Ay/+ mice (Fig. 3*B*), suggesting inhibition of inflammation and macrophage invasion into adipose tissue. Obesity is reportedly associated with macrophage infiltration of adipose tissue, which is likely to promote insulin resistance (27,28). Inhibition of macrophage invasion of adipose tissue may be involved in the higher insulin sensitivity and glucose tolerance observed in apoE$^{-/-}$;Ay/+ mice.

As described above, plasma adiponectin levels were increased in apoE$^{-/-}$;Ay/+ mice, suggesting normal adipocyte differentiation in vivo. Furthermore, mRNA expressions for adipocyte-related proteins, such as CCAAT/enhancer binding protein-α, peroxisome proliferator–activated receptor-γ, and aP2, were similar among adipose tissues from apoE$^{+/+}$;Ay/+, apoE$^{+/-}$;Ay/+, and apoE$^{-/-}$;Ay/+ mice (Fig. 3*C*). mRNA expressions levels of these three genes were also similar in adipose tissues from younger apoE$^{+/+}$;Ay/+ and apoE$^{-/-}$;Ay/+ mice, 4 weeks of age, when body weights were not significantly different (data not shown). In addition, apoE deficiency did not alter sterol regulatory element–binding protein 1 (SREBP1) expression (Fig. 3*C*). These findings indicate

that adipocytes are normally differentiated in apoE$^{-/-}$;Ay/+ mice in vivo.

Adenoviral apoE replenishment induced obesity and diabetes in genetically obese mice. To confirm that the metabolic phenotypes observed in apoE$^{-/-}$;Ay/+ mice were, in fact, mediated by apoE deficiency, we examined metabolic effects of adenovirus-mediated apoE expression in the livers of apoE$^{-/-}$;Ay/+ mice. Replenishment of apoE protein (human apoE3) resulted in markedly decreased plasma cholesterol, triglyceride, and FFA levels (Supplemental Fig. 2*A* [online appendix]), indicating functional expression of apoE. HPLC analyses of plasma lipid profiles revealed that adenoviral replenishment of apoE protein in apoE$^{-/-}$;Ay/+ mice markedly decreased the chylomicron and VLDL fractions (Supplemental Fig. 2*B* [online appendix]).

Increases in body weight for 7 days after adenoviral administration were significantly greater with the apoE adenovirus than with the LacZ control adenovirus (Fig. 4*A*). Liver weights tended to be increased (Fig. 4*B*), and those of brown adipose (Fig. 4*C*) and epididymal, mesenteric, and retroperitoneal white adipose (Fig. 4*D*) tissues were significantly increased with apoE adenoviral administration. Histological analyses revealed that apoE replenishment increased sizes of brown (Fig. 4*E* and *F*) and white (Fig. 4*G* and *H*) adipocytes. In addition, glucose tolerance tests revealed that apoE replenishment worsened glucose tolerance in apoE$^{-/-}$;Ay/+ mice (Fig. 4*I*). These findings show clearly that circulating apoE contributes to increased adiposity and the glucose intolerance associated with obesity. Furthermore, plasma leptin levels were significantly increased on day 7 after adenoviral administration. TNF-α and adiponectin levels tended to be increased and decreased, respectively (Fig. 4*J*), suggesting that circulating apoEs are involved in obesity-induced alterations in adipocytokine levels.

ApoE occurs in three major isoforms (apoE2, -E3, and -E4) in humans. ApoE3, the most common isoform, is considered to be the wild type. To compare the roles of the three human apoE isoforms in obesity and diabetes, recombinant adenoviruses encoding human apoE2 and -E4 as well as apoE3 were injected into apoE$^{-/-}$;Ay/+ mice. Administration of these apoE adenoviruses resulted in similar expression amounts of apoE proteins (data not shown), and similar increases in body weights (Supplemental Fig. 3*A* [online appendix]) and blood glucose levels (Supplemental Fig. 3*B* [online appendix]). These findings suggest that the three apoE isoforms contribute similarly to fat accumulation and glucose tolerance.

ApoE-less VLDL was uptaken into adipocytes, and the liver was impaired. Why does apoE deficiency inhibit obesity in genetically obese mice? We next examined the uptake of β-VLDL, with or without apoE, into fully differentiated 3T3-L1 adipocytes. β-VLDL obtained from apoE$^{-/-}$ mice was labeled with DiI, followed by incubation with or without recombinant human apoE3. As shown in Fig. 5*A*, uptake of apoE-deficient VLDL was markedly lower, by 85%, than that of apoE-positive (after incubation with human apoE3) VLDL. These findings suggest that impaired VLDL uptake into adipocytes contributes to decreased adiposity in apoE$^{-/-}$;Ay/+ mice. Thus, VLDL uptake into adipocytes is likely to play a role in excess fat deposition and, thereby, in the development of diabetes associated with obesity.

ApoE deficiency reportedly reduces hepatic VLDL secretion, resulting in fatty liver findings (11). In our model as well, hepatic triglyceride secretion was inhibited in apoE$^{-/-}$;Ay/+ mice compared with apoE$^{+/+}$;Ay/+ mice, by 48% (Fig. 5*B*). However, interestingly, apoE$^{-/-}$;Ay/+ mice displayed less fat accumulation in the liver than apoE$^{+/+}$;Ay/+ mice (Fig. 1*D–F*). To elucidate the underlying mechanism, we examined β-VLDL uptake into the liver. Fluorescence-labeled β-VLDL, with or without apoE, was intravenously injected into wild-type C57BL/6 mice. Fluorescence values in the liver were then measured. Uptake of apoE-deficient β-VLDL was markedly lower, by 49%, than that of apoE-positive VLDL (Fig. 5*C*). Thus, despite decreased secretion, decreased β-VLDL uptake with apoE deficiency may contribute to prevention of hepatic steatosis. Therefore, apoE is likely to be involved in excess fat uptake into hepatocytes as well as adipocytes. Taken together with the findings that adenoviral apoE replenishment decreased the VLDL fraction (Supplemental Fig. 2*B* [online appendix]), our results indicate that apoE-dependent VLDL transport into tissues, including the liver and adipose tissue, is involved in the development of obesity, resulting in glucose intolerance and insulin resistance.

ApoE deficiency decreased food intake and increased energy expenditure in genetically obese mice. Next, to elucidate the systemic mechanism underlying the obesity prevention associated with apoE deficiency, we first measured food intakes in apoE$^{+/+}$;Ay/+ and apoE$^{-/-}$;Ay/+ mice. Interestingly, apoE deficiency in Ay mice significantly suppressed food intake (Fig. 5*D*). Then, to eliminate the secondary effects of reduced food intake in apoE$^{-/-}$;Ay/+ mice, ApoE$^{+/+}$;Ay/+ mice were allotted the same amounts of food consumption as apoE$^{-/-}$;Ay/+ mice, followed by weight measurement and glucose tolerance testing. Pair-feeding blunted the body weight increments in apoE$^{+/+}$;Ay/+ mice, while the weights of pair-fed apoE$^{+/+}$;Ay/+ mice were significantly greater than those of apoE$^{-/-}$;Ay/+ mice (Fig. 5*E*). ApoE$^{-/-}$;Ay/+ mice exhibited better glucose tolerance than pair-fed apoE$^{+/+}$;Ay/+ mice (Fig. 5*F*). Thus, the inhibition of obesity and glucose intolerance by apoE deficiency is not attributable solely to decreased food intake.

Next, we measured basal metabolic rates. As shown in Fig. 5*G*, resting oxygen consumption in both the light and the dark phase at 5 weeks of age was significantly greater in apoE$^{-/-}$;Ay/+ than in apoE$^{+/+}$;Ay/+ mice. Taken together with the pair-feeding experiment results, these findings show that decreased food intake and increased energy expenditure both contribute to the prevention of obesity and insulin resistance with apoE deficiency and that apoE is involved in regulation of energy metabolism.

DISCUSSION

To examine the effects of apoE deficiency on insulin resistance associated with obesity, apoE$^{-/-}$ mice were interbred with KK-Ay mice. ApoE$^{-/-}$;Ay/+ mice showed resistance to the development of obesity and glucose intolerance. Insulin sensitivity was markedly greater in apoE$^{-/-}$;Ay/+ than in apoE$^{+/+}$;Ay/+ mice. Recently, several attempts to induce obesity in apoE$^{-/-}$ mice have been reported, but the results have been somewhat controversial (12–14). In the present study, in addition to inhibition of adiposity and insulin resistance with apoE deficiency, adenoviral apoE replenishment reversed inhibition of obesity and glucose intolerance. These findings directly demonstrate apoE involvement in the development of obesity and obesity-related disorders of glucose metabolism and insulin sensitivity. Chiba et al. (14) previously reported